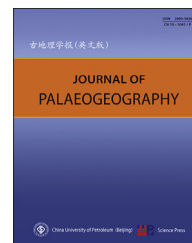




Available online at www.sciencedirect.com

ScienceDirect

journal homepage: <http://www.journals.elsevier.com/journal-of-palaeogeography/>



Facies analysis and sedimentary environments

Mammal-bearing Pleistocene deposits, Vranić, southwestern Pannonian Basin System



Adriano Banak^a, Zsófia Ruzsiczay-Rüdiger^b, Anita Grizelj^{a,*},
Martina Đuras^c, Krešimir Petrinjak^a, ASTER Team^{d,1},
Alexander Wieser^e, Monika Milošević^a, Davor Pavelić^f

^a Department of Geology, Croatian Geological Survey, Milana Sachsa 2, HR-10000 Zagreb, Croatia

^b Institute for Geological and Geochemical Research, HUN-REN Research Centre for Astronomy and Earth Sciences (MTA Centre of Excellence), Budaörsi Street 45, 1112 Budapest, Hungary

^c The Faculty of Veterinary Medicine, University of Zagreb, Heinzelova 55, HR-10000 Zagreb, Croatia

^d CEREGE, CNRS-IRD-Collège de France-INRAE UM34, Aix-Marseille Université, Aix-en-Provence, France

^e Faculty of Physics - Isotope Physics, University of Vienna, Währinger Straße 17, 1090 Vienna, Austria

^f Faculty of Mining, Geology and Petroleum Engineering, University of Zagreb, Pierottijeva 6, HR-10000 Zagreb, Croatia

Abstract Vranić site is a sand quarry that is located on the southern foothills of Papuk Mountain. From bottom to top of the succession, three sedimentary units have been recognized as: Unit 1 containing massive sand with scattered gravel-sized clasts, marl cobbles and boulders, and abundant marine mammal and fish fossils; Unit 2 consisting of sand intercalated with silt, clay and gravel, which may be horizontally bedded; and Unit 3, which is an erosionally-based lenticular matrix to clast-supported structureless gravel. The basal part of Unit 1 shows numerous reworked skeletal remains of Miocene marine mammals. Cosmogenic radionuclides constrain the age of burial of Unit 1 to 895 ± 211 ka, while the source area of Unit 1 had a quick denudation.

The massive sands deposited on the slopes of Papuk Mountain were vulnerable to erosion due to the absence of clay. Heavy rainfall or water from snow melting created flash floods that infiltrated the sands, thereby causing slope destabilization and deformation. This process led to slumps that were transformed into a sandy debris flow. This sediment was probably deposited during the interglacial marine isotope age (MIS) 21 period when the scarce vegetation and a warmer climate favored the melting of permafrost ice and consequently triggered slope movements during MIS 22. The reworked skeletal material sampled at the Vranić site comprises fossilized fish along with mammal bones and teeth. Thus, the Vranić site represents an important site for cetacean fossil remains and serves as an important data source for marine life in the Central Paratethys.

Keywords Miocene marine mammals, Alluvial slope deposit, Pleistocene, Cosmogenic nuclides, Pannonian Basin System

* Corresponding author.

E-mail address: agrizelj@hgi-cgs.hr (A. Grizelj).

Peer review under responsibility of China University of Petroleum (Beijing).

¹ Members of the ASTER Team: Georges Aumaitre (aumaitre@cerge.fr) and Karim Keddadouche (keddadouche@cerge.fr).

<https://doi.org/10.1016/j.jop.2024.04.001>

2095-3836/© 2024 The Author(s). Published by Elsevier B.V. on behalf of China University of Petroleum (Beijing). This is an open access article under the CC BY-NC-ND license (<http://creativecommons.org/licenses/by-nc-nd/4.0/>).

© 2024 The Author(s). Published by Elsevier B.V. on behalf of China University of Petroleum (Beijing). This is an open access article under the CC BY-NC-ND license (<http://creativecommons.org/licenses/by-nc-nd/4.0/>).

Received 16 January 2023; revised 21 May 2023; accepted 3 April 2024; available online 7 April 2024

1. Introduction

Vranić site is an abandoned sand pit located at the southern foothills of central Papuk Mountain in the North Croatian Basin, southwestern Pannonian Basin System (Fig. 1A and B). Its sandy sediments are transported from surrounding mountains (Krkalo, 1998). The sand deposition in the Pannonian Basin System during the Miocene and Pliocene is induced by regional tectonic events and repeated transgressions and regressions accompanied by intense weathering of exposed rocks in the source area (Pavelić, 2001). Such processes may cause downslope bulk movements of rock, soil and debris (Cruden, 1991).

Slides, slumps, and debris flows are the three basic types of subaerial mass movement processes. Landslides are caused by disturbances, such as seismic shock, snow and glacier melt, rainfall, erosional undercutting, major storms, and human activities; while the debris flows may result from individual landslides, but are also common on modern and ancient channelized alluvial fans at the adjoining area from mountains to valleys. Besides alluvial fans, debris flows also occur on non-channelized alluvial slopes that develop on steeply inclined mountain flanks (Hawley and Wilson, 1965; Smith, 2000; Kuhle and Smith, 2001). The major characteristic of the debris flow is unconsolidated slope material that is easily erodible, such as loose sand. In Central Europe, loose deposits affected by the mass movement have been identified in the Alps (Wetzels et al., 2006), Vienna Basin (Šujan et al., 2022) and Pécs-Danitzpuszta locality in the central Pannonian Basin System (Kazár, 2005, 2006; Sebe et al., 2020; Botfalvai et al., 2023). The latter location is a significant site demonstrating rich associations of reworked Miocene vertebrates related to mass movement processes. These associations, discovered along with marine mammal remains (whales and dolphins) at many localities in the Pannonian Basin System and the Vienna Basin, prove the existence of marine connection of the Central Paratethys with the World Ocean in the Middle Miocene (Müller, 1855; Mikuž, 1999; Kazár, 2006; Sabol et al., 2021; Botfalvai et al., 2023). The Vranić site is the only locality in the central North Croatian Basin from where the Middle Miocene fish and marine mammal associations have been reported

and considered as allochthonous fossils due to their scattering distribution in the sand deposit (*Rhomboidea* beds) (Jamičić et al., 1987; Vrsaljko et al., 2010; Banak et al., 2015).

This study has two principal aims: (1) to interpret the depositional mechanisms and the sedimentary environment, where the sand and reworked mammal remains accumulated similarly to the analogous site at Danitzpuszta in Hungary (Sebe et al., 2020; Botfalvai et al., 2023); and (2) to present a detailed description of fossil association for a better correlation of marine mammals with other similar finds in the Central Paratethys. This study strives to provide guidelines for finding undiscovered mammal fossil sites not only in the Pannonian Basin System but also in other regions with similar geological characteristics. Cosmogenic $^{26}\text{Al}/^{10}\text{Be}$ burial age dating has been performed to estimate the timing of sand deposition.

2. Geological setting

The deposition of the Pannonian Basin System initiated from the Lower Miocene. The evolution of this basin is characterized by a syn-rift phase of tectonic thinning of the crust and subsidence, followed by the successive Late Miocene post-rift phase marked by subsidence due to cooling of the thinned lithosphere (Royden, 1988; Horváth, 1995; Pavelić, 2001; Kováč et al., 2017; Šujan et al., 2021a). The post-rift phase is followed by the neotectonic phase during the Pliocene up to the Quaternary. In this phase, thermal subsidence stopped and the extension was replaced by compressional to transtensional tectonics resulting in basin inversion, which was expressed as large-scale folding of the Pannonian lithosphere with the coexistence of uplifting and subsiding areas (Fodor et al., 2005; Bada et al., 2007). Palaeogeographically, the Pannonian Basin System belongs to the Central Paratethys, which underwent Cenozoic evolution (periods of isolation and semi-isolation from the ambient seas during Miocene), utilizing the regional Neogene stages (Báldi, 1980; Rögl and Steininger, 1981; Piller et al., 2007; Kováč et al., 2018; Pavelić and Kovačić, 2018).

In the North Croatian Basin, the syn-rift phase lasted from the Early Miocene to the Middle Miocene (i.e., end of the middle Badenian according to the regional stages) and is characterized by a depositional

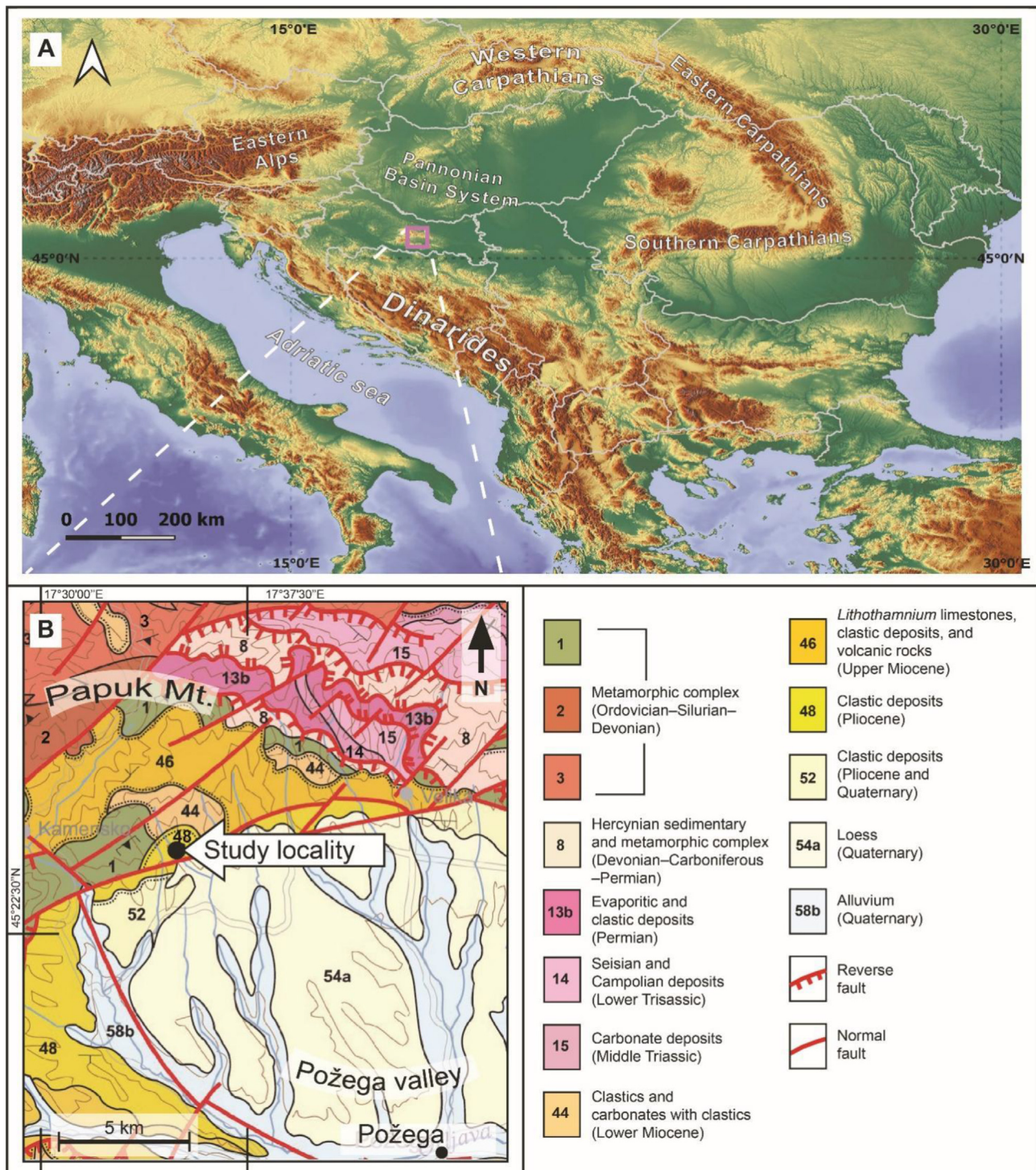


Fig. 1 A) Position of the Vranić site in the Pannonian Basin System; B) Simplified geological map of the area around the study locality (modified after CGS, 2009).

succession showing a transition from continental to fully marine, which is further controlled by extensional tectonics, climatic changes, and volcanic activity (Pavelić *et al.*, 1998, 2022). The Middle Miocene (i.e. late Badenian) to the Late Miocene post-rift phase is characterized by a quick and gradually ceasing

subsidence. It is expressed in the sedimentary record by a transition from marine to continental deposition when Lake Pannon was formed and consequently terminated by a short inversion event (Jamičić, 1995; Márton *et al.*, 1999; Pavelić, 2001; Tomljenović and Csontos, 2001; Šujan *et al.*, 2021b).

The final isolation of the Pannonian Basin System occurred at the start of the Late Miocene at 11.6 Ma (i.e. Pannonian) during the formation of the brackish Lake Pannon (Magyar, 1995; Piller *et al.*, 2007; Bakrač *et al.*, 2012; Magyar *et al.*, 2013; Kováč *et al.*, 2017; Pavelić and Kovačić, 2018; Sebe *et al.*, 2020). In the North Croatian Basin, Lake Pannon was gradually and diachronously filled up mostly by sand and silt, which were derived from the Eastern Alps and the Carpathians by a delta system prograding from the northwest and ending in the Early Pliocene (Saftić *et al.*, 2003; Kovačić and Grizelj, 2006; Sebe *et al.*, 2020). The lacustrine to deltaic deposits on Papuk Mountain are known as the Upper Miocene–Lower Pliocene *Rhomboidea* beds (Fig. 1B, legend codes 46 and 48), which are overlain by Pliocene–Lower Pleistocene *Viviparus* beds of lacustrine to fluvial origin (Kurečić *et al.*, 2021).

The *Rhomboidea* beds are characterized by moderate- to well-sorted sands mostly composed of quartz and feldspars, with a subordinate content of muscovite and fragments of metamorphic, magmatic and sedimentary rocks (Basch *et al.*, 1995; Ivković *et al.*, 2000; Vrbanac, 2002; Kovačić *et al.*, 2004; Kovačić and Grizelj, 2006; Matošević *et al.*, 2023). These petrographic properties are considered uniform in the North Croatian Basin (Jamičić *et al.*, 1987). In the Early Pliocene, the brackish Lake Pannon was locally substituted by the freshwater Lake Slavonia, which finally filled up during the Early Pleistocene (Mandić *et al.*, 2015; Pavelić and Kovačić, 2018; Kurečić *et al.*, 2021). Deposits of Lake Slavonia locally overlie the *Rhomboidea* beds in the Požega valley close to the southern slopes of Papuk Mountain (Fig. 1B: legend code 52) (Jamičić *et al.*, 1987). In the Pliocene–Quaternary neotectonic phase, the North Croatian Basin was affected by a strong tectonic compression that generated basin inversion and structural block uplifting (Jamičić *et al.*, 1987; Jamičić, 1995; Márton *et al.*, 1999; Pavelić, 2001; Tomljenović and Csontos, 2001), thereby resulting in the uplift and exhumation of the basement rocks of Papuk Mountain. The erosion of the Paleozoic–Mesozoic basement, syn-rift and post-rift deposits led to their deposition in the foothills.

3. Methods

3.1. Fieldwork

The Vranić site (45°25'49"N; 17°31'12"E; base elevation: 290 m a.s.l.; top elevation: 316 m a.s.l.) is located at the southern foothills of the central Papuk Mountain. The exposed wall of the sand pit is around 300 m long and 30 m thick. It strikes in the NE–SW

direction and is gently inclined towards the Požega valley. The sections were measured along the wall.

Fieldwork included detailed facies analysis and sampling for successive laboratory analyses. Three depositional units (Units 1, 2 and 3) were recognized and characterized by different sedimentary features, and separated by distinct depositional boundaries. The lithology, sedimentary structures, bed thickness and nature of bedding planes were recorded for all the lithounits. Grain size, mineralogical and petrographic analyses were performed on individual beds to determine the composition and reconstruction of the provenance of the clastic material.

Grain surface microtexture was classified by scanning electron microscopy (SEM). Sand samples were used for cosmogenic radionuclide (CRN) burial age determination, a method which has not been used before in the North Croatian Basin. Lastly, vertebrate fossils were characterized along with their stratigraphic, palaeoclimatic and palaeoecological implications.

3.2. Grain size analysis

Grain size analysis was performed on 23 sediment samples, while the sieving method was executed on 19 coarse-grained samples. A set of seven sieves (mesh widths 2.8, 1.25, 0.9, 0.45, 0.25, 0.125 and 0.09 mm) were used for the analyses, and grain size distributions were classified based on the Wentworth scale (Wentworth, 1922).

Grain size analysis of four fine-grained sediment samples (VR14–VR17) was performed on bulk samples using a Shimadzu Laser Diffraction Particle Size Analyzer SALD-2300. Dried samples (0.1 g) were isolated for analysis. The samples were treated with 4% Na₄P₂O₇·10H₂O and deionized water against coagulation and dispersed around 5 h on a shaker. Each measurement was repeated three times with a pump speed of 8 and a sonicator test (30 s). The average value of particle diameters was used for the grain size distribution.

3.3. Mineralogical analysis

The mineral composition of 16 samples from different segments of Units 1 and 2 was determined by polarized light microscopy analysis of heavy (HMF) and light mineral fractions (LMF) at grain size fractions of 0.063–0.16 mm using sodium polytungstate ($\rho = 2.8 \text{ g/cm}^3$). The ribbon counting method was used to determine the qualitative and quantitative composition of HMF and LMF, as described by Mange and Maurer (1992) on at least 300 grains per fraction.

3.4. Thin-section petrography

Thin-section petrography was carried out on four pebble samples of different lithologies (VR-B1, VR-B2, VR-B3 and VR-B4) from Unit 3 of Section B3 (Fig. 2). Canadian balsam was used as a binder and standard.

3.5. SEM

SEM was used to examine four samples of sand-sized particles ($>63 \mu\text{m}$) from Sections A and B1 of Unit 1. The samples having a thickness of 15 nm were coated with gold. More than 70 different grains were analyzed using a JEOL JSM 35CF model with a magnification range of 180–860 \times . The quartz grain surface microtexture classification method and terminology were followed after Mahaney (2002) and Vos et al. (2014).

3.6. Burial age determination using CRN

3.6.1. Theory

Burial age determination using *in situ* produced CRN considers the concentration and ratio of cosmogenic ^{26}Al and ^{10}Be in sedimentary quartz grains that were initially exposed and dosed and then shielded from cosmic radiation. The nuclide concentrations of sediment at the time of burial are variable, and depend on nuclide production rates and the denudation rate at the source area. However, the surface $^{26}\text{Al}/^{10}\text{Be}$ ratio is fairly constant (Granger, 2006; Granger and Riebe, 2014). Upon burial, the sediments are partly or completely shielded from cosmic rays. Thus, ^{26}Al and ^{10}Be are no longer produced and the $^{26}\text{Al}/^{10}\text{Be}$ ratio starts to decrease. This change in the

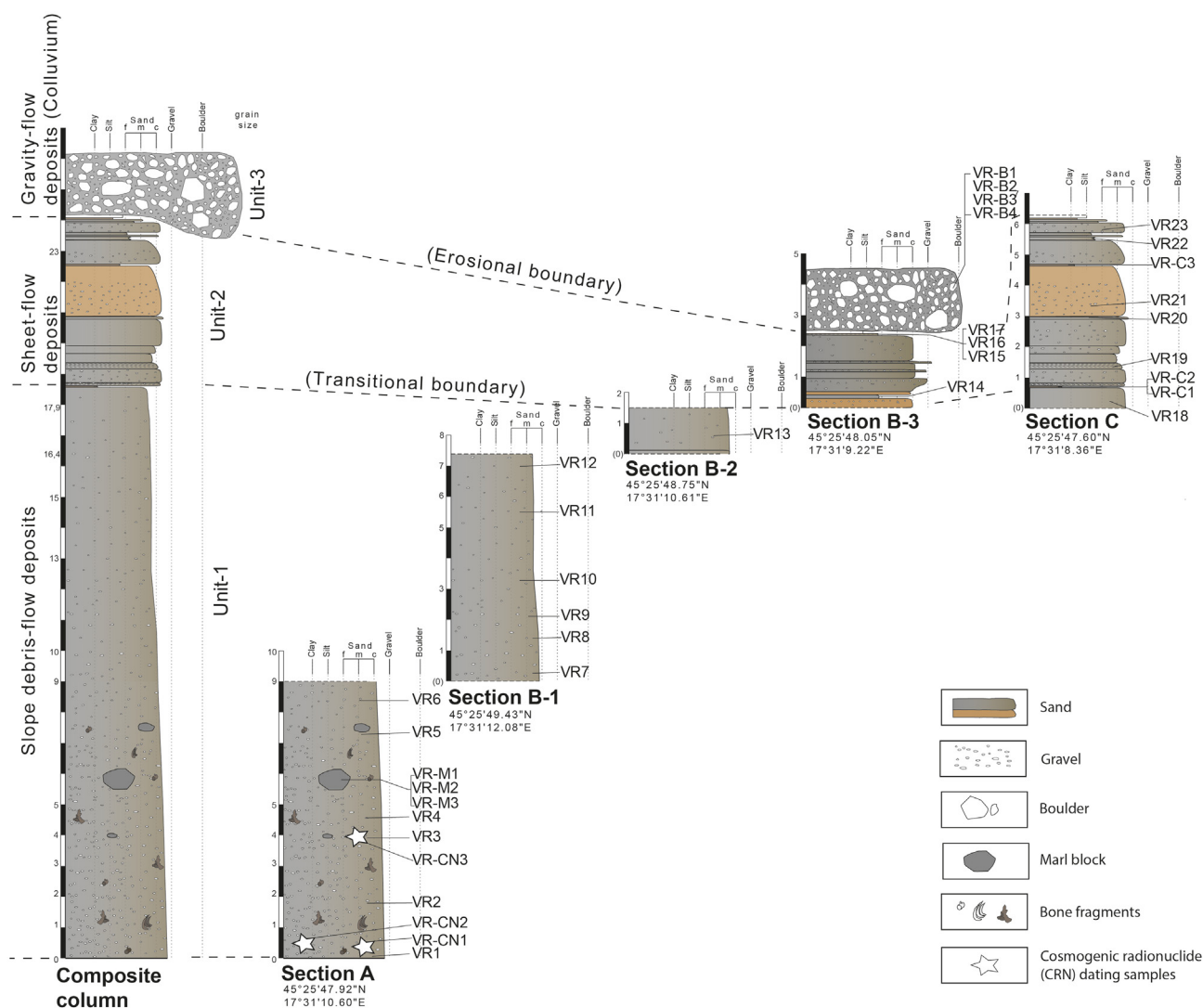


Fig. 2 A composite geological column combined from five laterally-correlated sections (A, B1, B2, B3 and C), showing the sedimentary characteristics and sampling positions in the Vranić site, southwestern Pannonian Basin System. VR1 to VR23: Samples for grain size analysis; VR-CN1 to VR-CN3 (asterisks): Samples for CRN burial age dating; VR-M1 to VR-M3, VR-B1 to VR-B4, and VR-C1 to VR-C3: Samples for modal analysis.

nuclide ratio allows the calculation of the burial duration of the sediment. More detailed methodology, constants and equations used for age calculations are presented in Supplementary CRN-1.1.

3.6.2. Sample collection and laboratory procedures

The lower part of the massive sand of Unit 1 was targeted for age determination of the deposition of the Vranić site sediments (Figs. 3 and 4). In 2016, two samples were taken for $^{26}\text{Al}/^{10}\text{Be}$ burial age determination (VR-CN1 and VR-CN2). These samples were processed and analyzed in 2017, which provided divergent results. An additional sample was collected in 2018 (VR-CN3) and processed together with new aliquots from previous samples. In 2020, measurements by accelerator mass spectrometry (AMS) for this sample batch were performed at sampling depths of 20.0 ± 0.5 m for VR-CN1, 19 ± 1.0 m for VR-CN2 and 15 ± 0.5 m for VR-CN3.

The bulk sand samples were sieved, and the 0.5–1.0 mm grain size was processed at the Cosmogenic Nuclide Sample Preparation Laboratory of the Institute for Geological and Geochemical Research (Budapest, Hungary; http://www.geochem.hu/kozmozgen/Lab_en.html) following the procedures by Brown *et al.* (1992), Merchel and Herpers (1999) and Merchel *et al.* (2019) as described in Ruszkiczay-Rüdiger *et al.* (2021). Stable ^{27}Al determination was performed by inductively coupled plasma-optical emission spectrometry (ICP-OES; ICAP 6500 from Thermo) at CEREGE, Aix-en-Provence, France (2017 sample batch) and microwave plasma atomic emission spectrometry (Agilent 4100 MP-AES) at the Institute of Nuclear Research, Debrecen, Hungary (2020 sample batch). Purified BeO and Al₂O₃ were mixed with Nb powder in a 1:4 ratio and with Ag powder in a 1:1 ratio, respectively. The targets were prepared for AMS measurement at the CEREGE, Aix-en-Provence, France (ASTER; Arnold *et al.*, 2010) (2017 sample batch) and at the Vienna Environmental Research Accelerator, Faculty of Physics, University of Vienna (VERA; Steier *et al.*, 2019) (2020 sample batch). The reported uncertainties comprise the analytical uncertainties, the uncertainty of the ^{10}Be and ^{26}Al half-lives, the spallation production rate of ^{10}Be , the $^{26}\text{Al}/^{10}\text{Be}$ spallation production rate ratio and sediment density (2.0 ± 0.2 g/cm³).

3.7. Micropaleontological analysis

Micropaleontological analysis was carried out on three samples from the marl block (VR-M1, VR-M2

and VR-M3) in Unit 1 of Section A. Approximately 300 g of sediment per sample was disaggregated by soaking in diluted H₂O₂ for 48 h, then washed through sieves (0.25, 0.125, 0.09 and 0.063 mm) and dried. Each dried residue was observed under a binocular microscope. Fossil remains (e.g. foraminifera, ostracods, and bryozoans) were hand-picked and determined.

3.8. Macropaleontological analysis

The sandy material from the base of Unit 1 was sieved at the outcrop using a 1 × 1 m sieve with a 2-mm mesh size. A total of 159 fossil individual bones were collected and cleaned. The macrofossil material was determined at the class level with special emphasis on cetacean fossils, which comprise skull bones, teeth, vertebrae, chevron bone and flipper bones. The nomenclature and measurements were done as per the methods of Kazár and Venczel (2003).

4. Results

4.1. Facies description

A composite log was made based on five individual sections (Fig. 2). The deposits are lithologically heterogeneous and comprise gravel, sand, silt, and clay. It is divided into three sedimentary units, i.e., Units 1, 2, and 3, from bottom to top. The sediment grains are distinctly fining upwards in Unit 1. Both Units 1 and 2 show poor sorting with the number and size of large gravels decreasing upwards. They differ significantly in silt fraction (averagely 1.07% in Unit 1 vs. 34.2% in Unit 2) and in gravel fraction (averagely 12.69% in Unit 1 vs. 2.9% in Unit 2). The sediment grain-size data are shown in Supplementary Table S1.

Unit 1

The measured thickness of this unit is about 19 m with its lower boundary unexposed. It comprises pale brown to light grey, poorly-sorted, loose, massive sands, scattered with pebble-, cobble- and boulder-sized gravels from the pre-Miocene basement (e.g., metagabbro and gneiss) and Middle Miocene marls (Table 1, Sm; Fig. 3D). It shows no stratification. The gravels are angular to subrounded, mostly 0.5–1.5 cm in size, occasionally reaching 2.5 cm, and mostly accumulate at the lower part of the unit (Figs. 2 and 3B, C; Supplementary Table S1). Comparatively, the

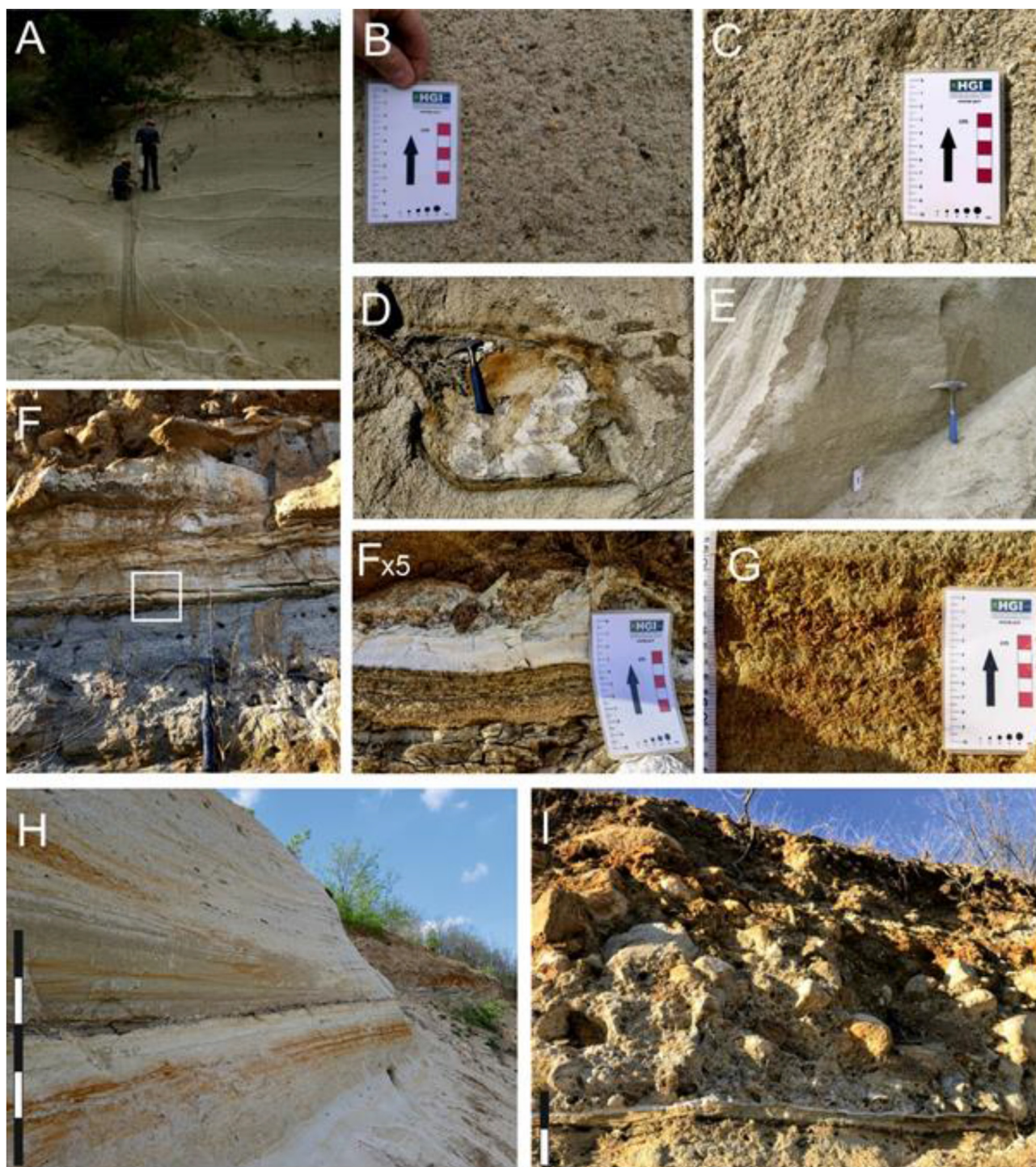


Fig. 3 Outcrop photographs showing the different facies in the Vranić site, southwestern Pannonian Basin System. A) The general overview of Section A (Unit 1, Sm), where the two persons can be observed in the middle part of the section, collecting gravelly sand samples; B) Pebbly sand in the upper part of Section A (Unit 1, Sm); C) Sand in the lower part of Section B1. It is gravelly and structureless (Unit 1, Sm); D) Marl block from the middle part of Section A (Unit 1, Sm); E) Pebbly sand in Section B2 (Unit 1, Sm); F) Intercalation of horizontally laminated sand with white clay in the lower part of Section B3 (Unit 2, Fl). The white rectangle shows the position of a detailed picture of layered sediment (F × 5); G) Pebbly and massive sand in the lower part of Section B3 (Unit 2, Sh); H) Horizontal bedding is a characteristic of Section C (Unit 2, Fsl). A thin grey clay bed is visible in the middle of the picture. Scale is 1 m; I) Upper part of Section B3 is characterized by a chaotic gravel composed of pebbles, cobbles and boulders (Unit 3, Gmc). Scale is 40 cm. For the position and lithological characteristics of the sections, see [Figs. 1 and 2](#). The hammer in the pictures for scale is 33 cm long.

Table 1 Facies description and interpretation of deposits from the Vranić site, southwestern Pannonian Basin System. Codes are modified after Miall (1996).

Unit	Facies or facies association	Code	Description	Interpretation
1	Structureless sand	Sm	Nearly 19-m-thick, pale brown to light grey, poorly-sorted sands, scattered with pebbles, cobbles, and boulders up to 150 cm long. The clasts are angular to subrounded, some containing a marine microfossil assemblage (i.e., scattered fossilized fish, and marine mammal bones and teeth) of Middle Miocene. Stratification or any other internal structure is absent. The Unit 1 contacts the Unit 2 with a transitional boundary.	Non-cohesive sandy debris flow
2	Intercalation of sand with clay, silt and gravel (i.e., intercalation forms a 2.5–6.15-m thick unit due to erosion by overlying Unit 3)	Sh	Horizontally bedded sand is coarse-grained and poorly sorted. Beds tabular, 5–164-cm thick. Grey to ochre or reddish. Bedding planes planar or slightly erosional. Scattered rounded clasts 0.3–0.6 cm in diameter. Normal or inverse grading.	Sandy sheet floods
		Sm	Structureless pebbly sand is fine- to coarse-grained and poorly sorted. Beds 10–87 cm thick. Lower bedding planes are irregular.	Non-cohesive sandy debris flow
		Fl	Interbedded sand, silt and clay form small units of 5–25 cm thick. Well-developed horizontal lamination. Silt and clay are grey or white in color.	Lower flow regime traction currents and suspended-load fallout from very weak currents
		Gh	Horizontally bedded gravel is clast- to matrix-supported. Gravel clasts are subrounded, 1–5 cm in diameter. Sandy matrix. Greyish to brownish. Two tabular beds 5- and 32-cm thick.	Unconfined gravelly sheet floods
		Fsl	Intercalation of clay/silty clay. Two horizontally bedded and laminated layers 4–6 cm thick, grey. Lower bedding planes are flat, and upper bedding planes are sharp and erosional.	Suspended-load fallout from weak currents
3	Structureless gravel	Gmc	Poorly sorted matrix to clast-supported lenticular gravel. Composed of rounded pebbles and cobbles and subangular to angular boulders up to 100 cm long. Matrix is poorly sorted mixture of sand, silt, clay and soil. The maximum thickness of the lens is 200 cm.	Sediment-gravity deposits (colluvium)

upper part of the unit is mostly made of coarse sands (0.2–0.5 mm in size; Fig. 3E). Marl clasts and blocks are frequent with variable dimensions, where the largest ones are 150 cm long (Figs. 2 and 3D) and were found at the 6 m level in Section A. The marl clasts contain a marine Middle Miocene (Badenian) microfossil assemblage, numerous single scattered fossilized fish and marine mammal bones, teeth and bone fragments (Fig. 2). The grain size analysis (Supplementary Table S1) shows a marked dominance of sand-sized fraction (average 86.23%) in the Unit 1, compared to the gravel content (average 12.69%) and the silt-sized fraction (average 1.07%). Clay fraction is absent in this unit.

Interpretation

Unit 1 is interpreted to be deposited from non-cohesive sandy debris flow, as indicated by the sand-dominated composition, lack of any regular internal structures (Table 1, Sm), low content or lack of fine-grained material, poor to very poor sorting, and scattered pebble- and boulder-sized clasts up to 150 cm long (Dott Jr, 1963; Nemeč and Steel, 1984; Miall, 1996; Shanmugam, 1996). The 19-m-thick unit indicates that the debris flow was probably generated by subaerial gravitational mass movements, i.e. landslides on the sand-rich hill slope. The heavy mineral composition of this unit indicates a local source of

sediments, such as the Paleozoic metamorphic rocks and the Middle Miocene marine deposits (Fig. 1B). The mammalian fossils found as isolated fragments in the sand without their original coating of Middle Miocene marl, suggest a period of reworking before being incorporated into the debris flow.

Unit 2

Unit 2 is lithologically heterogeneous. It mainly comprises sands, intercalated with clays, silts and gravels. Horizontal beddings and laminations are developed, some of which pinch out laterally (Fig. 3F, F × 5). Five facies have been distinguished: horizontally bedded sand (Table 1, Sh), structureless pebbly sand (Table 1, Sm), interbedded sand and silt (Table 1, Fl), horizontally bedded gravel (Table 1, Gh) and two horizontally bedded layers of grey clay/silty clay (Table 1, Fsl). Horizontally bedded, mostly coarse-grained, poorly sorted sand prevails throughout the unit (Fig. 3H). Beds are tabular and 5–164 cm thick, where thick and very thick beds comprise amalgamated layers. The colors of the beds vary from grey to ochre or red. The bedding planes are planar or slightly erosional. Rounded pre-Miocene basement clasts of 0.3–0.6 cm in diameter are scattered through the deposits. Some beds show normal or inverse grading. Pebbly sand occurs at the lower and middle parts of the unit as 10–87 cm thick brownish beds. The sands are fine-to coarse-grained and poorly sorted. The lower bedding planes are irregular. Intercalations of sand, silt and clay in the form of tabular beds occur throughout the unit with varying thicknesses of 5–25 cm (Fig. 3F). The intercalations show well-developed horizontal lamination up to a few millimeters thick. Silt and clay are grey or white.

Horizontally bedded gravel is represented in the middle and upper parts of the unit by two single tabular beds with the thickness of 5 cm and 32 cm, respectively. They have irregular lower bedding planes. The gravel is clast-to matrix-supported with a sandy matrix and vary in the shades of grey to brown (Fig. 3G). Gravel clasts are subrounded and comprise the pre-Miocene basement, mainly 1–1.5 cm in diameter. Two distinct horizontally laminated layers of clay/silty clay are present at the lower and upper parts of Section C (Fig. 3H). Both layers are grey and 4–6 cm thick and consist of flat lower bedding planes and sharp erosional upper contacts.

The thickness of this unit varies laterally from 2.5 m to 6.15 m. The results of the grain size analysis (Supplementary Table S1) reveal that sand dominates in Unit 2 (50.1%), however not as notable as in Unit 1, and this unit has significant silt (34.2%). The average

clay content is 12.8%, and the gravel fraction has an average of 2.9%. The lower boundary of Unit 2 is transitional, whilst the upper boundary is reflecting the erosional base of overlying Unit 3.

Interpretation

Horizontally bedded sand beds (Table 1, Sh) are interpreted as deposited from rapidly running water in the upper flow regime, such as sandy sheet floods occurring within alluvial environments (Smoot, 1983; Blair, 1999; Nemeč and Kazancı, 1999), as indicated by the tabular geometry of beds, erosional lower boundaries, medium-to good-sorting and scattered pebbles. The sheet floods represent discharge probably due to strong rainfall or snow melting combined with the absence of channelized drainage. Normal grading is probably a result of waning floods, whereas inverse grading can be interpreted as a consequence of a gradual increase in flow velocity due to heavy rainfall. Amalgamated units can be related to prolonged or repetitive periods of run-off. The ochre and reddish colors of the sand probably reflect pedogenetic processes. The pebbly sand beds (Table 1, Sm) that are similar to deposits of Unit 1 are likewise interpreted as deposited from non-cohesive sandy debris flows.

The horizontally laminated sand intercalated with clay and silt (Table 1, Fl) represents lower flow regime subaqueous traction deposits. On the other hand, the clay and silty clay (Table 1, Fsl) reflect suspended-load fallout from very weak currents in ephemeral ponds, which formed on the slope-toe (Smoot, 1983; Platt and Keller, 1992; Miall, 1996). Pedogenesis probably resulted in the brownish-to-ochre color of the laminated sand. The tabular geometry of the horizontally bedded gravel beds (Table 1, Gh), their clast to matrix support, pebbles up to 5 cm diameter, and lack of basal erosion exhibit deposition generated by laterally expanded unconfined gravelly sheet floods resulting from rapid drainage of a large volume of water on the hill slope after heavy rainfall (Bull, 1972; Galloway and Hobday, 1996; Mutti *et al.*, 1996). Poor sorting infers deposition fairly close to the source area (Lewis and McConchie, 2012).

Unit 3

Unit 3 comprises a lenticular matrix to clast-supported, structureless gravel (Table 1, Gmc). The clasts are very poorly sorted and include pebbles, cobbles and boulders (Fig. 3I). Light brown, beige and grey are the predominant shades of color of the sediments in this unit. Unit 3 forms the top of the succession with the maximum thickness of 200 cm. The

pebbles are rounded, mostly 5–20 cm in diameter, whilst the boulders are subangular to angular and up to 100 cm long. The gravel is polymictic, which is represented by different bedrock lithologies derived from the pre-Miocene basement and Middle Miocene marine deposits. The matrix is a very poorly sorted mixture of sand, silt, clay and soil. The boundary to underlying Unit 2 is erosional.

Interpretation

The chaotic internal texture of the gravel (Table 1, Gmc), very poor sorting and erosional and oversized boulders reveal that the facies represents a clastic slope waste material deposited by sediment-gravity processes in the lower part of the hill, i.e. colluvium (Holmes, 1965; Blikra and Nemeč, 1998; Šujan *et al.*, 2019). The polymictic clast composition and small sand content show that the main source was the pre-Miocene basement and Middle Miocene marine deposits. This abrupt change in provenance probably indicates a new sedimentary cycle that is not genetically related to Units 1 and 2. This might also indicate a much longer age gap between Units 2 and 3 than between Units 1 and 2.

4.2. Mineralogical composition

The mineral composition of sand is very similar throughout the entire succession. The LMF is dominated by quartz (61%–85%) and feldspars (8%–27%) with scarce rock fragments (1%–12%). Angular quartz grains with undulose extinction predominate, whilst those with uniformity are rarer. K-feldspar is more common than plagioclase (Supplementary Table S2). Among the K-feldspar grains, microcline can be recognized by the typical cross-hatched twinning. The grains are mostly fresh and angular, but also altered grains are kaolinized and sericitized. Schists with a low degree of metamorphism and quartzite-type particles are the most common rock fragments, whereas chert is rarer (Supplementary Table S2). Muscovite is present sporadically (Supplementary Table S2). In HMF, translucent minerals are dominant (56%–78%). Opaque minerals are moderately present (22%–36%), while chlorite rarely occurs.

Among the opaque minerals, ilmenite predominates. The most abundant translucent heavy minerals in all samples are epidote, zoisite-clinozoisite and garnet (Supplementary Table S2). Tourmaline, rutile zircon, apatite, amphibole and staurolite are less abundant or in trace amounts in the analyzed samples. Pyroxenes and kyanite are present only in few samples. Within almost all these different types of minerals,

corroded, irregularly broken, rounded and euhedral grains are also present (Fig. 4). Epidotes are yellow green to pale green in color (Fig. 4A–F). Garnets are transparent or pale pink. Unweathered, euhedral and subhedral grains are common, whereas rounded grains occur rarely (Fig. 4G–I). Zircon exhibits three morphological types: rounded (Fig. 4J), subhedral (Fig. 4K) and euhedral forms (Fig. 4L and M). Rutile is reddish or orange in color and commonly of subhedral morphology (Fig. 4N–P). Staurolite is yellow to pale yellow and has distinctive slightly corroded grains (Fig. 4R and S). Sphene grains are mostly corroded (Fig. 4T). Tourmaline is light brown to dark brown, showing characteristic pleochroism. Euhedral grains are common (Fig. 4U), although irregular, corroded grains also occur. Kyanites are characterized by subhedral grains (Fig. 4V). Apatite is characterized by weakly rounded subhedral grains (Fig. 4W). Amphiboles are typical light green to brownish corroded grains (Fig. 4Z).

4.3. Petrography of pebbles, cobbles and boulders

Clasts from Unit 3 (Fig. 2) VR-B1 and VR-B2 consist of retrograde-metamorphosed gneiss–phyllonite (Fig. 5A and B). VR-B3 is a Badenian biocalcarenite as shown by the fossil association; prevailing red algae [*Lithothamnium* sp.], nonionids [*Cibicides* sp.], planktonic foraminifera and echinoid spines (Fig. 5C). Terrigenous, angular and subangular quartz grains are rarely present. The matrix is microsparite (Fig. 5). VR-B4 is metagabbro (Fig. 5D).

Cobbles of Badenian biocalcarenites and Pannonian clayey limestones predominate, along with the cobbles of retrograde metamorphism, namely phyllonite and metagabbro. Metamorphic cobbles belong to the Papuk metamorphic complex of pre-Variscan and early Variscan orogeny (Jamičić, 1983).

4.4. SEM results

SEM was used to analyze four sand-sized samples from Unit 1 (Sections A and B1), viz., VR-2, VR-6, VR-10 and VR-12 (Fig. 2). More than 80% of all grains from all four samples are angular or subangular (Fig. 6), whilst a small percentage of grains (>5%) are very angular. The rest are subrounded. Almost all grains have multiple fracture faces separated with sharp edges (Fig. 6). More than 50% of the grains display conchoidal fractures, while approximately 30% of the grains have subparallel linear fractures on their surfaces (Fig. 6). Linear and arc-shaped steps are detected on grain surfaces in all the samples, but

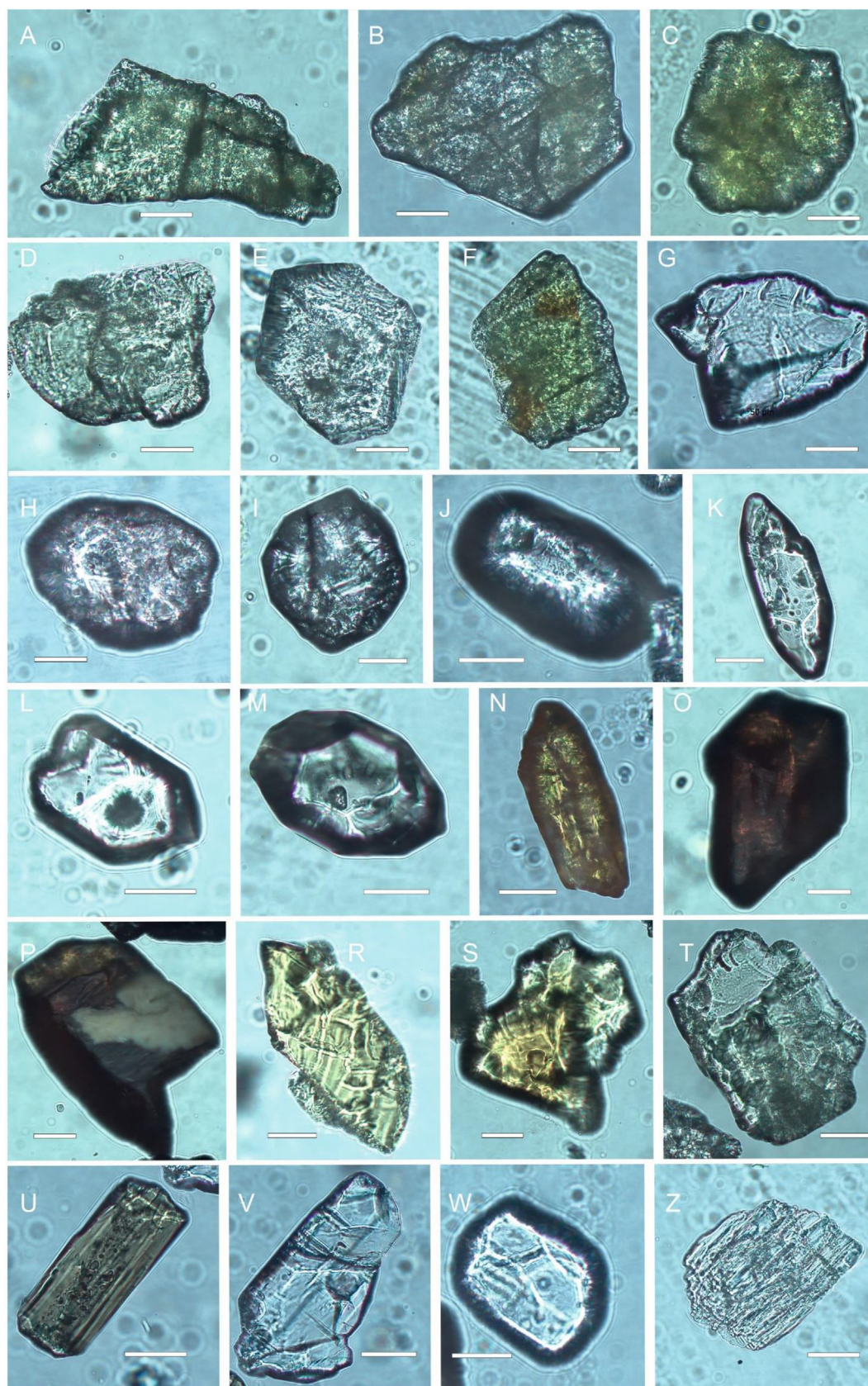


Fig. 4 Photomicrographs showing morphologies and corrosion of the studied minerals. A–D) Early to slightly corroded epidote; E) Euhedral epidote; F) Slightly corroded epidote; G) Unweathered garnet; H) Rounded garnet; I) Euhedral garnet; J) Rounded zircon; K) Subhedral zircon; L, M) Euhedral zircon; N–P) Subhedral rutile; R) Unweathered, slightly corroded staurolite; S) Corroded staurolite; T) Corroded sphene; U) Euhedral tourmaline; V) Subhedral kyanite; W) Subhedral apatite; Z) Corroded amphibole. All scale bar length = 50 μm .

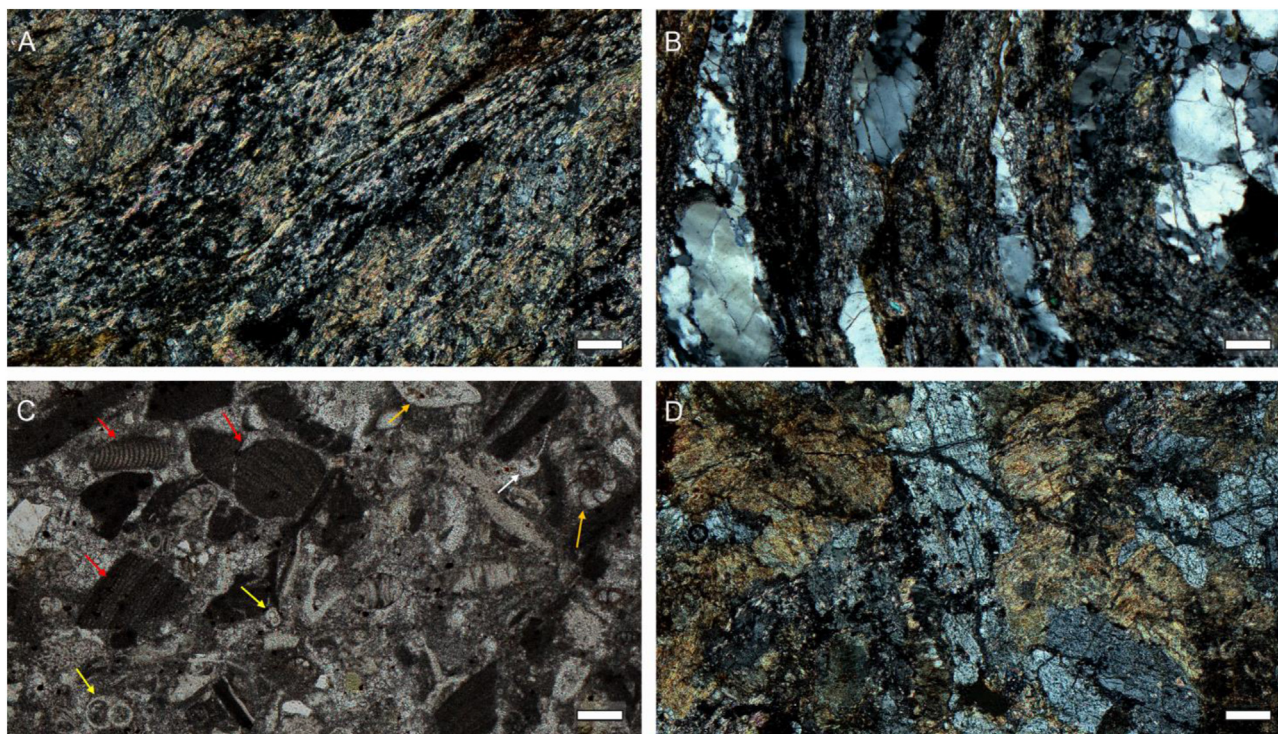


Fig. 5 A) Photomicrographs showing phyllonite (retrograde-metamorphosed gneiss) from VR-B1. N +; B) Phyllonite from VR-B2. N +; C) Biocalcarenes of Badenian age from VR-B3, with fossil fragments of red algae (*Lithothamnium* sp.; red arrows), echinoid spine (white arrow), benthic foraminifera (probably nonionids, *Cibicides* sp.; orange arrows), and planktonic foraminifera (yellow arrows). N +; D) Metagabbro from VR-B4. N +. All scale bar length = 0.2 mm.

they are visible on approximately 20% of the scanned grains. Medium-to high-relief grains dominate in all samples, with scarcity of the low relief ones. Most of the grains are elongated. Adhering particles are visible on almost all the grains (Fig. 6) and are probably an effect of drainage in porous, sandy sediment.

4.5. Cosmogenic nuclide dating

4.5.1. Measurement results

Supplementary Table S3 lists the laboratory parameters and measurement results for each sample.

The measured isotope ratios of both nuclides (^{26}Al and ^{10}Be) were very low in all samples ($^{10}\text{Be}/^9\text{Be}$: between 1.9×10^{-14} and 3.5×10^{-14} ; $^{26}\text{Al}/^{27}\text{Al}$: between 1.3×10^{-14} and 3.2×10^{-14}). In the 2016 batch (processed in 2017), the uncertainties of the ^{26}Al concentrations are high (20%–30%). Due to the low nuclide ratios, the blank correction for ^{10}Be was also high (19%–31%) but that for ^{26}Al was lower (2%–6%). The $^{10}\text{Be}/^9\text{Be}$ ratios of the process blank for the 2017 and 2020 sample batches were $(4.39 \pm 0.67) \times 10^{-15}$ and $(6.31 \pm 0.85) \times 10^{-15}$, respectively. The $^{26}\text{Al}/^{27}\text{Al}$

ratios of the blanks for the 2017 and 2020 sample batches were $(4.62 \pm 3.28) \times 10^{-16}$ (machine blank) and $(1.70 \pm 0.72) \times 10^{-15}$ (process blank), respectively.

Moreover, the calculated ^{10}Be and ^{26}Al concentrations were very low, and the derived $^{26}\text{Al}/^{10}\text{Be}$ ratios showed a diverse picture, from 2.79 ± 0.31 to 5.47 ± 1.76 (Supplementary Table S4). Both the highest and lowest values belonged to the measurements of VR-CN1 (coded as VR-CN1/17 and VR-CN1/20). Additionally, the uncertainty of the ^{26}Al concentration of VR-CN1/17 was unusually high (32%) (Fig. 7, therefore was considered as outliers and not used for further modelling. The results of the two measurements of the VR-CN2 sample were in agreement; thus, the weighted average ^{10}Be and ^{26}Al concentrations were calculated and used for the age modeling (VR-CN2/m; Supplementary Table S4). The VR-CN3 sample provided similar results to VR-CN2 within uncertainties (Supplementary Tables S3 and S4; Fig. 7).

4.5.2. Burial age calculations

The source rocks of the sediment deposited at Vranić site are Middle Miocene shallow marine

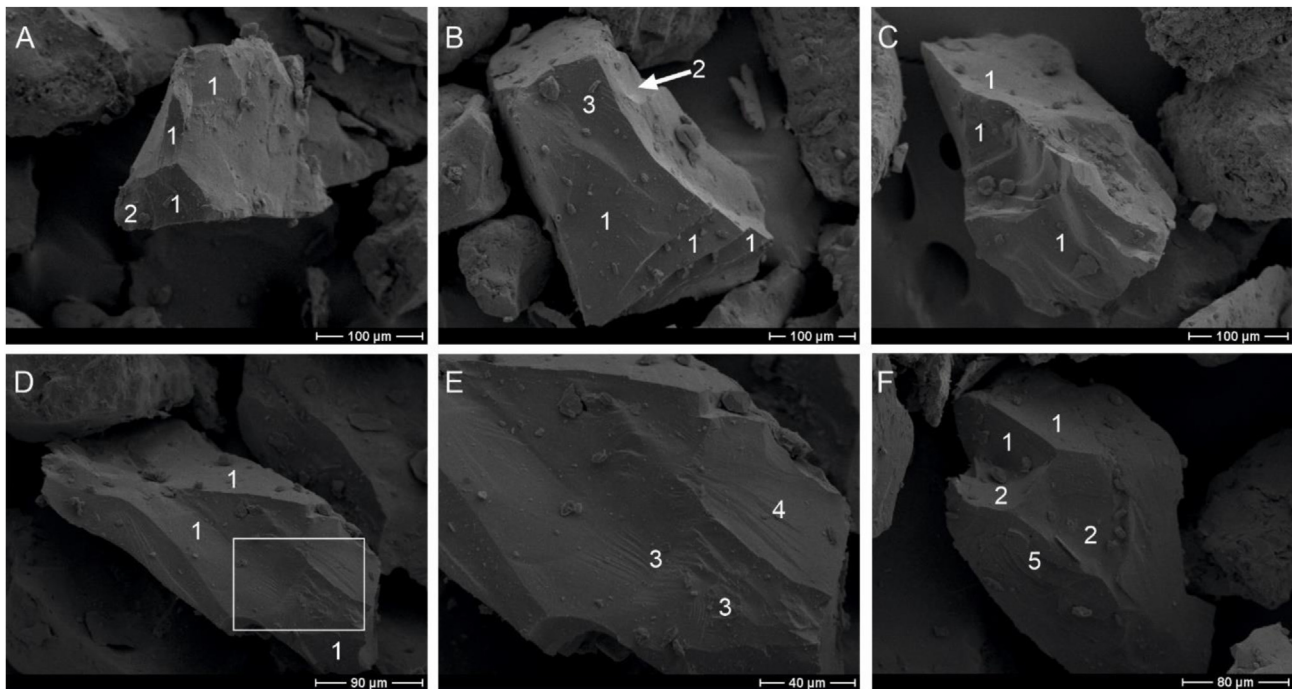


Fig. 6 SEM images of quartz and sand grains extracted from samples within Sections A and B1 of Unit 1. Typical microtextures and features: 1: Fracture faces; 2: Conchoidal fractures; 3: Subparallel linear fractures; 4: Linear steps; 5: Arc-shaped steps. A) Angular grain with sharp edges and medium relief. Fracture faces and conchoidal fracture are visible; B) Angular grain with sharp edges, fracture faces, conchoidal fracture and subparallel linear fractures; C) Subangular grain with fracture faces; D) Grain with sharp edges and medium to low relief. Magnification of the grain surface marked with a white rectangle; E) Subparallel linear fractures and linear steps visible on the enlarged surface of the grain; F) Subangular grain with sharp edges, fracture faces, conchoidal fractures and arc-shaped steps.

deposits. Because of the old age ($>>9$ Ma) of the sediment source, any CRN from the time before its sedimentation has decayed, thus the inherited CRN inventory (N_0 , see eq (1) in Supplementary CNR-1.1) has been neglected during the burial age calculation.

The burial durations and pre- and post-burial denudation rates were calculated using constants and equation (1) described in Supplementary CNR-1.1. Age calculation was performed using inverse modelling by solving equation (1) for burial age together with pre- and post-burial denudation rates simultaneously. Iterations by Chi2 minimization were repeated until the best model fit to the data was found. The resulting uncertainties included the analytical uncertainties as well as the uncertainties of the production rates and production rate ratios, ^{10}Be and ^{26}Al half-lives, sediment density and 10% uncertainty due to the uncertain subsurface depth of the samples.

The burial durations of VR-CN2/m and VR-CN3 were calculated at first, assuming complete burial, to be 1.05 ± 0.22 and 1.25 ± 0.20 Ma, respectively. Next, using the measured sample depth, the burial ages were calculated to be 0.60 ± 0.14 and 1.38 ± 0.34 Ma, respectively (Supplementary Table S4). The results are

sensitive to the sample depth, and the estimate is not in agreement. The assumption of complete burial ignores the fact that at 15–20 m depth, the muogenic CRN production might be considerable. The calculation with the current sample depth did not consider the recent surface truncation above the quarry, which was suggested by field evidence and by the divergent burial ages of the two samples at the measured sample depth.

Lastly, inverse modelling was performed, with the same age and denudation rate for both samples. To find the most probable thickness of removed material, the depth of recent truncation was increased from 0 m (measured sample depth) to 5 m in 1 m steps. The best model fit was achieved at 3 m recent surface truncation, with a burial duration of 895 ± 211 ka, a pre-burial denudation rate of 518 ± 122 m/Ma and a post-burial denudation rate of 113 ± 27 m/Ma (Supplementary Table S4). This burial age is considered the most probable age of the deposition of the Vranić sedimentary body, being the oldest dated Quaternary deposit in the southwestern Pannonian Basin System. The CRN burial age of ~ 900 ka documents a much younger depositional age of the Unit 1 sands than

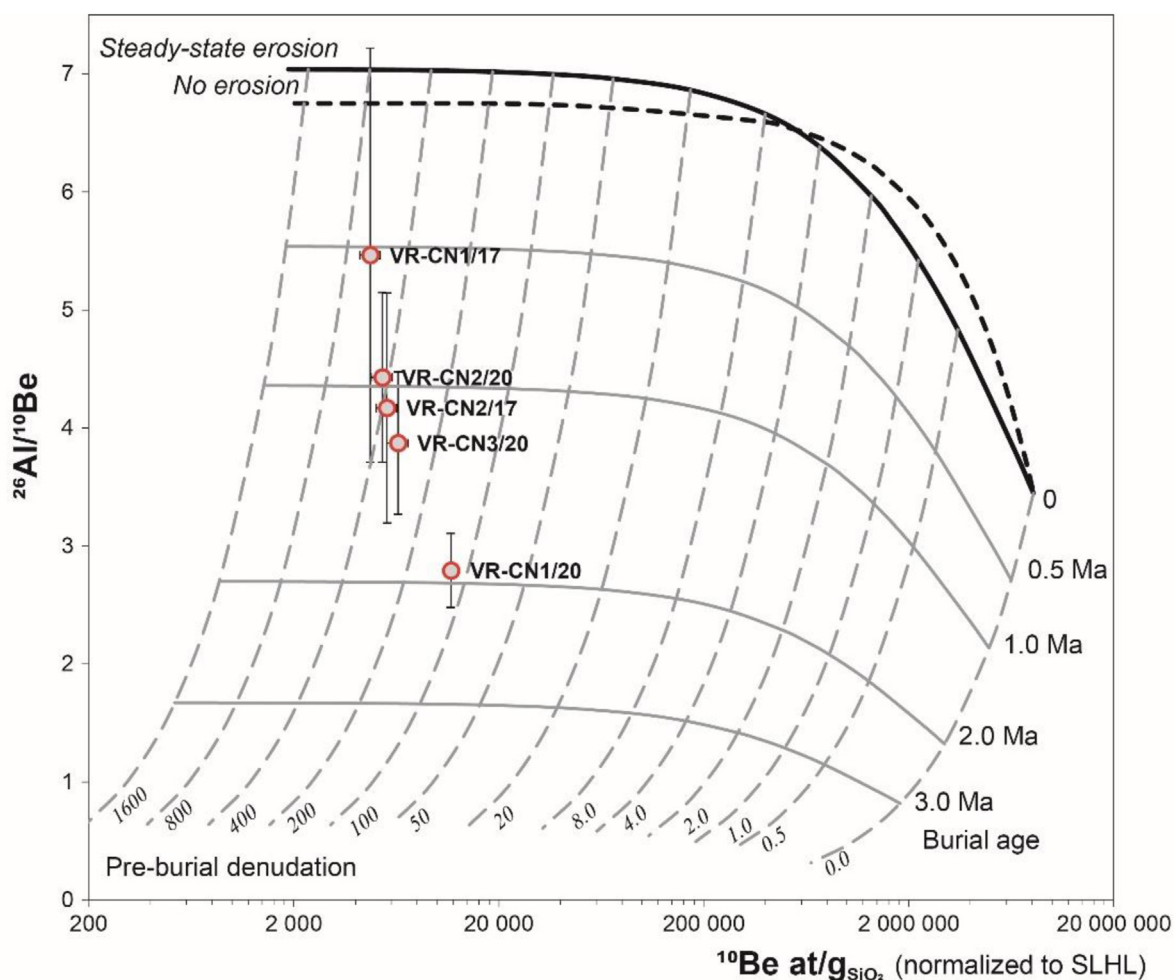


Fig. 7 Exposure–burial diagram of the measured nuclide concentrations (scenario of the complete burial). Note that all the samples are on the left side of the plot, in the range of fast pre-burial denudation rate (thin, dashed grey curves) and between 0.5 Ma and 2 Ma burial durations (thin, grey curves parallel with the uppermost, bold line of steady-state erosion at the surface (zero burial age)). Both VR-CN1 samples were treated as outliers and excluded from further data interpretation.

previously considered (the latest Miocene age - *Rhomboidea* beds; Jamičić *et al.*, 1987; Vrsaljko *et al.*, 2010; Banak *et al.*, 2015).

4.6. Paleontology

The microfossil assemblage is different for each fraction. The large fraction (125 μm sieve) contains lenticulinids (*Lenticulina orbicularis*, *L. calcar*, *L. austriaca* and *L. inornata*), *Planularia moravica*, *Vaginulina legumen*, *Siphonodosaria consobrina*, *Laevidentalina elegans*, *Nonion commune* and *Melonis pompilioides*. The middle fraction (90 μm sieve) contains the aforementioned species along with *Elphidium macellum*, *Orthomorphina* sp., *Globobulimina pyrula*, *Amphicoryna hispida*, *Sphaeroidina bulloides*,

Bulimina buchiana, *Cibicidoides ungerianus*, *Uvigerina semiornata*, *Islandiella punctata*, *Bolivina scalprata* var. *retiformis* and *Grigelis pyrula*. Badenian planktonic foraminifera includes *Globigerina bulloides*, *G. praebulloides*, *G. diplostoma*, *Trilobatus trilobus*, *Orbulina suturalis* and *Globoturborotalia bykovae*. Other fossils include spine fragments from echinoderm spines, *Bolboforma* sp., ostracods, fish skeleton and bryozoan fragments.

The osteological material consists of 159 fossils. Based on gross morphological characteristics, 78 fossilized bones and teeth, along with 81 fossilized bone fragments were identified. Fossilized bones and teeth came from fishes and mammals; out of these, 14 bones and 1 tooth belong to the order of whales (Fig. 8). The cetacean bones were represented by 5



Fig. 8 Cetacean fossils sifted from the sand. A–E) Humerus; F, I, J) Ulna; G) Phalanx; H) Tooth; K) Radius; L) Petrous; M) Tympanic and part of the temporal bone; N, O) Vertebra.

humeri, 1 radius, 3 ulnas, 1 phalanx, 2 vertebrae, 1 tympanic part of the temporal bone and 1 petrous part of the temporal bone (Fig. 8). According to gross morphology and size, these remains possibly originated from the toothed whale (suborder Odontoceti) of the polyphyletic assemblage Kentriodontidae (Marx *et al.*, 2016).

5. Discussion

5.1. Provenance and causes of mass movements and sediment-gravity processes

The debris flows, sheetflood and pond deposits reflect the evolution of a relatively short-lived sandy terrestrial environment, where deposits of Units 1 and 2 accumulated (Fig. 9). The low CRN concentrations with the estimated high pre-burial denudation rates infer rapid erosion of the source area. This depositional association is characteristic of an alluvial fan environment that usually forms along the margins of uplifted structural blocks bounded by faults with significant dip-slip. Different processes may trigger

various depositional mechanisms, e.g., sediment-gravity flows, tractional currents and suspended-load fallout (Hooke, 1967; Heward, 1978; Nemec and Steel, 1984; DeCelles *et al.*, 1991; Nemec and Postma, 1993). Since the presence of a distinctive alluvial fan or channelizing in the Vranić site has not been reported in the literature yet, the depositional environment is interpreted as an alluvial slope at the foot of a steeply inclined mountain (cf. Hawley and Wilson, 1965; Smith, 2000; Kuhle and Smith, 2001).

The dominant surface features on all grains are fracture faces, as shown in the SEM images of sand grains from Unit 1 (Fig. 6). This feature is typical of grains originating from mass wasting deposits resulting from slope movements (Mahaney *et al.*, 1991; Mahaney, 2002). Additionally, the absence of V-shaped percussion marks and microfeatures characteristic of fluvial transport (Mahaney, 2002), excludes the possibility of longer fluvial transport. Colluvial gravels of Unit 3 reflecting a new depositional cycle, indicate additional exhumation and strong erosion of the bedrock and steepening of the mountain slope where sediment-gravity processes operated. There are different ways to trigger sediment-gravity flow

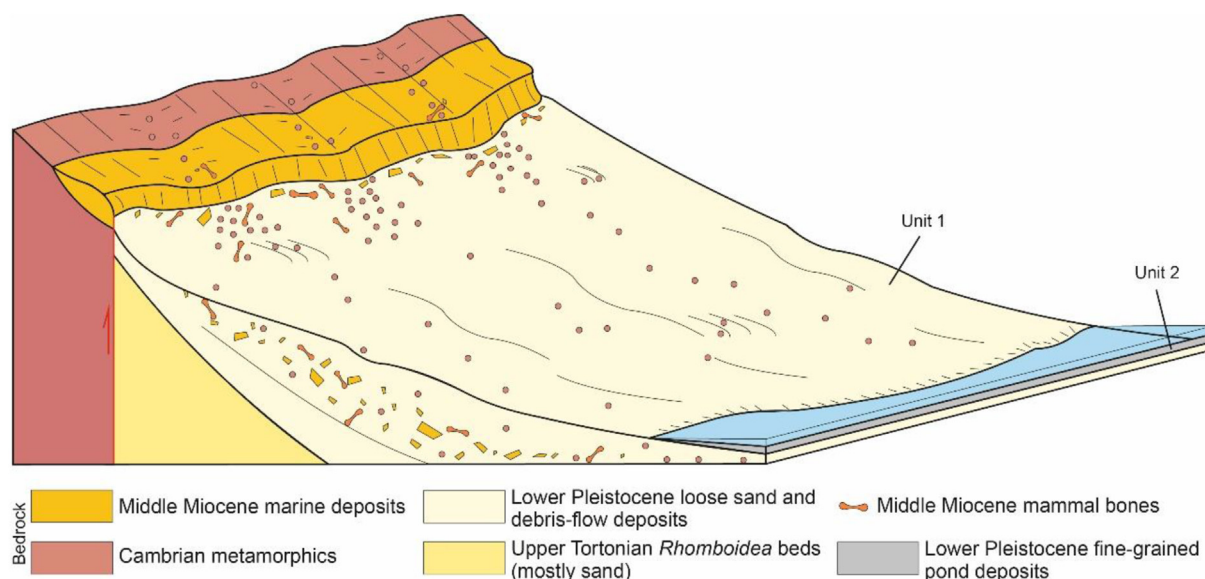


Fig. 9 Block diagram showing the depositional model of Units 1 and 2. After the mass movement that generated the debris flow (Unit 1), the sand-rich alluvial slope was stabilized and a pond was formed (Unit 2). Cambrian metamorphic rocks partly overlain by Middle Miocene deposits including marine mammal and fish fragments represented uplifting bedrock and were the source of coarse-grained material.

processes affecting the alluvial slope. Sands from Units 1 and 2 are mostly coarse-grained and usually have no fine-grained matrix. Pronounced angularity, sharp edges and non-weathered fractures of the analyzed grains from Unit 1 evidence short-distance transportation (Fig. 6). The origin of the sand is predominantly related to the pre-Miocene metamorphic basement. Moreover, the mineral composition of the sand indicates that only a limited part of the grains are of igneous and sedimentary origin (Fig. 4).

A metamorphic origin is distinctly indicated by quartz grains with undulose extinction and rock fragments (schists and quartzites) in LMF, along with epidote mineral group, garnet, amphibole, and staurolite and kyanite in HMF. The Paleozoic complex of metamorphic rocks is located in the basement of the Neogene and Quaternary deposits of Papuk Mountain (Figs. 1 and 5) as well as in the immediate hinterland of the Vranić site (Jamičić *et al.*, 1987; CGS, 2009). The mineral composition of the sand also reveals a smaller part of the grains to be of igneous and sedimentary origin. Therefore, euhedral zircons indicate an origin from igneous rocks, probably from the granitoids of the Papuk Mountain (Jamičić *et al.*, 1987). However, the rounded grains of ultra-stable minerals such as zircon, tourmaline and rutile (ZTR) indicate a sedimentary origin of a smaller part of detrital material. In general, these sands contain a small amount of ultra-stable ZTR minerals (Supplementary Table S2), while there are significantly prevalent unstable minerals, such as

amphibole, and moderately stable minerals, such as the epidote group and garnet. The weak chemical weathering of the detritus is indicated by the presence of weakly resistant minerals, such as amphibole and apatite, and by significant amounts of feldspars and prevailing angular grains, suggesting that the sands are mineralogically and structurally immature, indicative of short transport. The beds are homogeneous and consist mostly of sand with subordinate contents of gravel, silt and clay. Smaller amounts of sandy sediment could also originate from the *Rhomboidea* beds. The erosion probably caused the recycling of these deposits that resulted in an admixture of sand with a higher quartz content and better sorting than the sand of metamorphic origin. The combination of surface features detected on the sand grains, viz., conchoidal fractures, linear steps and arc-shaped steps, supports the interpretation of a multi-phased transport mechanism during several cycles of deposition terminating as gravitational transport as the final step in sedimentological evolution (Fig. 6). Also, recycling affected the Middle Miocene marine deposits (exposed at the surface), which are present in the form of big marl blocks in Unit 1.

The erosion of these marl blocks caused the separation of fish and marine mammal fossil fragments and whole fossil bones by the bedrock. Based on the present foraminifera index fossils *Vaginulina legumen*, *Bolivina scalprata subsp. muscosa*, *B. scalprata var. retiformis* and planktonic foraminifera *Orbulina*

suturalis, the marl samples from Unit 1 can be stratigraphically attributed to the lower Badenian (Cicha *et al.*, 1998). This determines the age of fossil remains and suggests a correlation between the source of the sediments with the Middle Miocene (lower Badenian) marine deposits in the North Croatian Basin.

The first mechanism to cause sediment formation in Units 1 and 2 is the uplift related to compressional tectonics affecting the North Croatian Basin in the Quaternary (Jamičić *et al.*, 1987; Jamičić, 1995; Márton *et al.*, 1999; Pavelić, 2001; Tomljenović and Csontos, 2001). The uplift of Papuk Mountain and the structural blocks bounded by steeply dipping faults, resulted in slopes mantled by thick sand accumulations. These tectonic processes triggered fault reactivation and associated seismic shocks integrated with the slope instability assisted by the changing climate, caused deformation and recycling of the Miocene deposits (Horváth, 1995; Pavelić, 2001; Tomljenović and Csontos, 2001; Šujan *et al.*, 2019).

Sands on the uplifted slope of Papuk Mountain were more vulnerable to erosion due to the lack of cohesive bonding between grains. Floods transporting these sediments indicate the existence of a large amount of water, with climate as a second mechanism responsible for the sediment formation in Units 1 and 2. Heavy rainfall and/or water produced by snow and permafrost melting could create flash floods that crossed and infiltrated into the sands, causing slope destabilization and deformation. This phenomenon led to the slumps, which were transformed into sandy debris flow due to liquefaction or dilatancy on the alluvial slope (Ellen and Fleming, 1987; McKenna *et al.*, 2012). The incision of the ephemeral or permanent water flow in the neighboring Požega valley could also have played a significant role in the destabilization of slopes mostly comprising loose sand, causing mass movements and deposition of Unit 1. Indeed, the mass movement might be generated by a combination of synsedimentary tectonics and humid climate, which generated the water and slope destabilization.

5.2. Depositional age

The burial age of 895 ± 211 ka of Unit 1 by modelling provides the most probable time of the deposition of the Vranić sediments. The low measured cosmogenic ^{26}Al and ^{10}Be concentrations coupled with $^{26}\text{Al}/^{10}\text{Be}$ ratios around 4 are also indicative of rapid erosion of the source area before sediment burial of Unit 1 (Fig. 7; Supplementary Tables S3 and S4).

The study revealed a hiatus between Units 2 and 3. The depositional age and duration of the hiatus as well as the thickness of the sedimentary pile removed by erosion

from the top of Unit 2 before the deposition of Unit 3 are unknown. This introduces an unambiguity in the subsurface depth of the samples, which means an additional uncertainty in the modelled CRN age and denudation rates. The burial ages were modelled using the measured sample depth, considering the recent surface truncation with a stepwise increase of the truncation depth up to the best model fit (described in Section 4.5). This was achieved in the scenario of the recent removal of 3 m of sediment with a calculated burial duration of 895 ± 211 ka, coupled with a valid approximation of the CRN burial age relevant for Unit 1. No further erosion events were taken into consideration for age calculation, as the above-listed unknowns for any additional scenarios introduced in our model would have added comparatively much larger uncertainty to the results than the present simplistic interpretation.

5.3. Early Pleistocene climate

The deposition of Unit 1 at 895 ± 211 ka coincides with the Middle Pleistocene Transition (MPT; 1.25–0.7 Ma; Clark *et al.*, 2006). It is characterized by the prolongation and intensification of glacial–interglacial climate cycles that intensified ~900 ka years ago (Maslin and Brierley, 2015). Elderfield *et al.* (2012) have considered this event to represent a global reorganization of the climate system. MIS 22 was the first long-term Pleistocene glaciation (Ehlers and Gibbard, 2007; Hernández-Almeida *et al.*, 2012).

Thick sandy loess deposits, represented as loess L9 in northern Eurasia, occurred during the MIS 24–MIS 22 transition (Dodonov, 2005), whilst in the Italian Alps, valley glaciers reached their earliest Pleistocene maximum southwards expansion during MIS 22 (Muttoni *et al.*, 2007). The synchronous occurrence of the least weathered thick loess unit L9 (corresponding to MIS 24–MIS 22) in Serbia and China suggests that climate change triggered the depositional event recorded by the Vranić sediments during the MPT that was a common feature in the Northern Hemisphere (Song *et al.*, 2018).

Precise determination of whether the deposition of sediments from Unit 1 occurred under interglacial or glacial climate conditions is impossible. Hence, interpreting the climatic conditions prevailing during the slope movement is difficult. The fact that the massive sand from Unit 1 contains numerous fragments of fossils and marl blocks (all Badenian age) indicates strong erosion just before deposition. Therefore, it is assumed that sediment deposition occurred under interglacial climate, possibly during the transition from MIS 22 to MIS 21, when a warm climate favored melting of ground ice accumulated during the first major glacial event.

5.4. Significance of marine mammal fossils

Complete, eroded and fragmented bones and teeth are the fossils found at Vranić site, which were derived from the marine fauna of the Central Paratethys (Fig. 8). Different whale species have been abundant and widely spread in the Central Paratethys, but the taxonomic gaps of ancient whales inhabiting this sea still remains unresolved. The remnant of both baleen whales (suborder Mysticeti) and toothed whales (suborder Odontoceti) have been identified by previous researchers. A preliminary study has shown that Vranić site represents a remarkable source of fossils with an estimated number of 20 fossils per 1 m³ (Vrsaljko *et al.*, 2010), with 9.4% (N = 15) out of the sampled fossils (N = 159) representing cetacean remains.

If bone fragments that cannot be determined to the order level are excluded, the ratio of cetacean fossils is even higher, representing 19.2% of all sampled fossils (N = 78). In this study, all cetacean fossils sampled in Vranić site originated from odontocetes, probably the kentriodontid taxa. Kentriodontidae is a summary term for a probable polyphyletic assemblage of generally small, Late Oligocene to Late Miocene dolphins not clearly assignable to any of the established delphinid families. Many kentriodontids are likely members of the superfamily Delphinoidea (Marx *et al.*, 2016).

The fossil remains of Odontoceti from the Middle Miocene of the Central Paratethys have been found in Tășad, Romania (Kazár and Venczel, 2003; Kazár, 2006), Domașnea, Romania (Codrea and Seretan, 2004), Cluj-Napoca, Romania (Kazár, 2006), Comănești, Romania (Grigorescu and Kazár, 2006; Kazár, 2006), Rohrbach, St. Margarethen, Kaisersteinbruch, Loretto, Bruck Neudorf and Vienna, Austria (Kazár, 2006), Kovácsszénája and Danitzpuszta, Hungary (Kazár, 2005) and Vranić site (Vrsaljko *et al.*, 2010) and Našice, Croatia (Japundžić *et al.*, 2017). The Croatian Natural History Museum in Zagreb, Croatia (Sanja Japundžić, Croatian Natural History Museum, Zagreb, pers. comm. 2022) hosts 137 cetacean fossils from Vranić site, whilst the Department of Anatomy, Histology and Embryology at the Faculty of Veterinary Medicine, University of Zagreb, Zagreb, Croatia, hosts another 78 cetacean fossils. Over the past decades, Vrsaljko *et al.* (2010) has reported the collection of more than 500 cetacean fossils at Vranić site.

6. Conclusions

The sands of Units 1 and 2 at the Vranić site are mineralogically and structurally immature sediments, originating from local rocks, which were mainly low-

grade metamorphic rocks, and in lesser quantity granitoids from Papuk Mountain. The increased relief caused by the uplift, which was triggered by compressional tectonics combined with fault reactivation. The seismic activity played an important role in the enhanced erosion and sediment remobilization on the flanks of the Papuk Mountain, along with heavy rainfall, and/or permafrost, and snow melting resulting in slope destabilization and flash floods, all of which resulted in slumps and sandy debris flows. This led to slope undercutting by the incising streams, further favoring slope destabilization and resulting in mass movements.

Numerous fragments of Badenian fossils and marl blocks were contained in the massive sands of Unit 1, indicating strong erosion before deposition. From the results of CRN data, this erosion occurred around the Early to Middle Pleistocene boundary. This climate-induced mechanism occurred at the beginning of an interglacial stage, possibly MIS 21. Therefore, tectonics and climate change simultaneously created the slope upliftment and accommodation space for the eroded sands. These driving forces also caused excess humidity and scarcity of vegetation, thereby triggering debris flows, which resulted in deposition of the sands of Units 1 and 2. In Unit 3, the disorganized, poorly sorted, erosionally based gravel with outsized boulders indicated clastic slope waste material or colluvium. The polymict clast composition and poor sand content indicated that the main source was a pre-Miocene basement belonging to the Papuk Mountain metamorphic complex of pre-Variscan and early Variscan orogeny, along with the Middle Miocene marine deposits. An abrupt change in provenance recorded by Unit 3 reflects a new depositional cycle, indicating additional exhumation and strong erosion of bedrock in the source area, and steepening of the mountain slope where sediment-gravity processes occurred. Investigation of the fossil remains from Vranić site led to the conclusion that all cetacean fossils sampled in Unit 1 originated from odontocetes, probably kentriodontids. Henceforth, this study shows that Vranić site is an important source of fossils for reconstructing the Paratethys cetofauna and marine life in Central Paratethys during the Middle Miocene.

Funding

This research was supported by Projects no. 181-181 1096 1093 of the Croatian Ministry of Science, Education and Sports and by the project NKFIH 124807 of the National Research, Development and Innovation Office of Hungary. The measurements performed at ASTER (CEREGE, Aix-en-Provence, France) were

supported by the INSU/CNRS, the French Ministry of Research and Higher Education, IRD and CEA. AMS measurements performed at VERA were supported by the RADIATE project 19001688-ST under the Grant Agreement 824096 from the EU Research and Innovation programme HORIZON 2020.

Availability of data and material

All data generated or analyzed during this study are included in this published article and its supplementary information file.

Authors' contributions

AB initiated the research and is the conceptual originator of the manuscript. He participated in field research, designed the structure of the article, interpreted the results of grain-size and SEM analysis, and participated in the determination of facies. He participated in the writing of all chapters, created Figs. 3, 5, 6 and Supplementary Table S1.

ZRR participated in field research and collection of samples for the cosmogenic nuclide burial dating method. She did the laboratory sample processing of the samples and interpreted the data obtained by the mentioned method and participated in the writing of all chapters. She created Fig. 7, Supplementary Tables S3 and S4.

AG participated in field research and taking samples for mineralogical analysis. She interpreted the data of the aforementioned analysis and participated in the writing of all chapters. She created Fig. 4 and Supplementary Tables S2.

MĐ interpreted the macropaleontological samples and participated in the writing of chapters 3, 4 and 5. She created Fig. 8.

KP participated in field research, sample collection and facies interpretation. He participated in the writing of chapters 4 and 5 and created Figs. 1 and 2.

ASTER Team Members GA and KK carried out the Accelerator Mass Spectrometry measurements of $^{10}\text{Be}/^9\text{Be}$ and $^{26}\text{Al}/^{27}\text{Al}$ ratios of the 2017 cosmogenic nuclide sample batch at ASTER.

AW performed the Accelerator Mass Spectrometry measurements of $^{10}\text{Be}/^9\text{Be}$ and $^{26}\text{Al}/^{27}\text{Al}$ ratios of the 2020 cosmogenic nuclide sample batch.

MM performed the analysis of the micropaleontological samples and participated in the writing of chapters 3 and 4.

DP participated in the writing of all chapters and interpretation of the facies. He created Fig. 9 and Table 1.

All authors read and approved the final manuscript.

Conflicts of interest

This manuscript has not been published and is not under consideration for publication elsewhere. We have no conflicts of interest to disclose. All authors listed made substantial contributions to this submission and approved the final version of the manuscript.

Acknowledgements

We are thankful to Silke Merchel and Peter Steier for their contribution to the AMS measurements at VERA. We are grateful to Mihály Braun for the MP-AES measurements carried out at the Institute of Nuclear Research, Debrecen, Hungary. We would like to thank Koraljka Bakrač and Mirko Belak for the preliminary palynological and petrographical analysis, Tomislav Kurečić for grain-size analysis on laser diffractometer and Radovan Avanić for fieldwork. We are very grateful to Michal Šujan and Finn Surlyk for their valuable reviews which improved the quality of the manuscript. We also thank the Associate Editors-in-Chief, Yuan Wang and Santanu Banerjee, and Handling Editor, Xiu-Fang Hu, for their review of the manuscript, which greatly improved its quality.

References

- Arnold, M., Merchel, S., Bourlès, D.L., Braucher, R., Benedetti, L., Finkel, R.C., Aumaître, G., Gottsdang, A., Klein, M., 2010. The French accelerator mass spectrometry facility ASTER: Improved performance and developments. *Nuclear Instruments and Methods in Physics Research Section B: Beam Interactions with Materials and Atoms*, 268(11), 1954–1959. <https://doi.org/10.1016/j.nimb.2010.02.107>.
- Bada, G., Horváth, F., Dövényi, P., Szafián, P., Windhoffer, G., Cloetingh, S., 2007. Present-day stress field and tectonic inversion in the Pannonian Basin. *Global and Planetary Change*, 58, 165–180. <https://doi.org/10.1016/j.gloplacha.2007.01.007>.
- Bakrač, K., Koch, G., Sremac, J., 2012. Middle and Late Miocene palynological biozonation of the south-western part of Central Paratethys (Croatia). *Geologia Croatica*, 65(2), 207–222.

- Báldi, T., 1980. A korai Paratethys története. *Földtani Közlöny*, 110, 456–472.
- Banak, A., Đuras, M., Avanić, R., Grizelj, A., Posilović, H., 2015. Neogene marine mammals from Vranić sand deposit [Poster]. In: Horvat, M., Wacha, L. (Eds.), *Book of Abstracts*. Hrvatski geološki institut, Zagreb, p. 24.
- Basch, O., Pavelić, D., Bakrač, K., 1995. Gornjopontski faciyesi sjevernog krila Konjšćinske sinklinale kod Huma Zabočkog (Hrvatsko zagorje). In: Vlahović, I., Velić, I., Šparica, M. (Eds.), *First Croatian Geological Congress, Proceedings*, pp. 57–61.
- Blair, T.C., 1999. Sedimentology of the debris-flow-dominated Warm Spring Canyon alluvial fan, Death Valley, California. *Sedimentology*, 46(5), 941–965. <https://doi.org/10.1046/j.1365-3091.1999.00260.x>.
- Blikra, L.H., Nemeč, W., 1998. Postglacial colluvium in western Norway: Depositional processes, facies and palaeoclimatic record. *Sedimentology*, 45(5), 909–959. <https://doi.org/10.1046/j.1365-3091.1998.00200.x>.
- Botfalvai, G., Kocsis, L., Szabó, M., Király, E., Sebe, K., 2023. Preliminary report on rare earth element taphonomy of a Miocene mixed age fossil vertebrate assemblage (Pécs-Danitzpuszta, Mecsek Mts., Hungary): Uptake mechanism and possible separation of palaeocommunities. *Historical Biology*, 35(4), 498–517. <https://doi.org/10.1080/08912963.2022.2049771>.
- Brown, E.T., Brook, E.J., Raisbeck, G.M., Yiou, F., Kurz, M.D., 1992. Effective attenuation lengths of cosmic rays producing ^{10}Be and ^{26}Al in quartz: Implications for exposure age dating. *Geophysical Research Letters*, 19(4), 369–372. <https://doi.org/10.1029/92GL00266>.
- Bull, W.B., 1972. Recognition of alluvial-fan deposits in the stratigraphic record. In: Rigby, K.J., Hamblin, W.K. (Eds.), *Recognition of Ancient Sedimentary Environments*. *SEPM Special Publications*, 16, 63–83.
- CGS, 2009. Geological Map of Republic of Croatia. *M 1:300.000*. Croatian Geological Survey, Department for Geology, Zagreb.
- Cicha, I., Rögl, F., Rupp, C., Ctyroka, J., 1998. Oligocene–Miocene Foraminifera of the Central Paratethys. *Abhandlungen Der Senckenbergischen Naturforschenden Gesellschaft*, 549, 1–15.
- Clark, P.U., Archer, D., Pollard, D., Blum, J.D., Rial, J.A., Brovkin, V., Mix, A.C., Piasias, N.G., Roy, M., 2006. The middle Pleistocene transition: Characteristics, mechanisms, and implications for long-term changes in atmospheric $p\text{CO}_2$. *Quaternary Science Reviews*, 25(23), 3150–3184. <https://doi.org/10.1016/j.quascirev.2006.07.008>.
- Codrea, V., Seretan, V., 2004. A middle Miocene dolphin from Domasnea (Caransebeş-Mehadia Miocene basin). *Studia Universitatis Babeş-Bolyai: Geologia*, 49(2), 3–10. <https://doi.org/10.5038/1937-8602.49.2.1>.
- Cruden, D.M., 1991. A simple definition of a landslide. *Bulletin of the International Association of Engineering Geology*, 43(1), 27–29. <https://doi.org/10.1007/BF02590167>.
- DeCelles, P.G., Gray, M.B., Ridgway, K.D., Cole, R.B., Pivnik, D.A., Pequera, N., Srivastava, P., 1991. Controls on synorogenic alluvial-fan architecture, Beartooth Conglomerate (Palaeocene), Wyoming and Montana. *Sedimentology*, 38(4), 567–590. <https://doi.org/10.1111/j.1365-3091.1991.tb01009.x>.
- Dodonov, A.E., 2005. The stratigraphic transition and suggested boundary between the early and middle Pleistocene in the loess record of northern Eurasia. In: Head, M.J., Gibbard, P.L. (Eds.), *Early–Middle Pleistocene Transitions: The Land–Ocean Evidence*. *Geological Society of London, Special Publication*, 247, 209–219. <https://doi.org/10.1144/GSL.SP.2005.247.01.11>.
- Dott Jr, R.H., 1963. Dynamics of subaqueous gravity depositional processes. *AAPG Bulletin*, 47(1), 104–128.
- Ehlers, J., Gibbard, P.L., 2007. The extent and chronology of Cenozoic Global Glaciation. *Quaternary International*, 164–165, 6–20. <https://doi.org/10.1016/j.quaint.2006.10.008>.
- Elderfield, H., Ferretti, P., Greaves, M., Crowhurst, S., McCave, I.N., Hodell, D., Piotrowski, A.M., 2012. Evolution of ocean temperature and ice volume through the mid-Pleistocene climate transition. *Science*, 337(6095), 704–709. <https://doi.org/10.1126/science.1221294>.
- Ellen, S.D., Fleming, R.W., 1987. Mobilization of debris flows from soil slips, San Francisco Bayregion, California. In: Costa, J.E., Wieczorek, G.F. (Eds.), *Debris Flows/Avalanches: Process, Recognition and Mitigation*. *GSA Reviews in Engineering Geology*, 7, 31–40. <https://doi.org/10.1130/REG7-p31>.
- Fodor, L., Bada, G., Csillag, G., Horváth, E., Ruzkiczay-Rüdiger, Z., Palotás, K., Sikhegyi, F., Timár, G., Cloetingh, S., Horváth, F., 2005. An outline of neotectonic structures and morphotectonics of the western and central Pannonian Basin. *Tectonophysics*, 410(1), 15–41. <https://doi.org/10.1016/j.tecto.2005.06.008>.
- Galloway, W.E., Hobday, D.K., 1996. *Terrigenous Clastic Depositional Systems: Applications to Fossilfuel and Groundwater Resources*, second ed. Springer, New York, pp. 1–485.
- Granger, D.E., 2006. A review of burial dating methods using ^{26}Al and ^{10}Be . *GSA Special Papers*, 415, 1–16.
- Granger, D.E., Riebe, C.S., 2014. Cosmogenic nuclides in weathering and erosion. In: Holland, H.D., Turekian, K.K. (Eds.), *Treatise on Geochemistry, Volume 5: Surface and Ground Water, Weathering, and Soils*, second ed. Elsevier Science Ltd., Amsterdam, pp. 401–436.
- Grigorescu, D., Kazár, E., 2006. A new Middle Miocene odontocete (Mammalia: cetacea) locality and the Sarmatian marine mammal event in the Central Paratethys. *Oryctos*, 6, 53–68.
- Hawley, J.W., Wilson, W.E., 1965. *Quaternary geology of the Winnemucca area, Nevada*, 5. University of Nevada Desert Research Institute Technical Report.
- Hernández-Almeida, I., Sierro, F.J., Cacho, I., Flores, J.A., 2012. Impact of suborbital climate changes in the North Atlantic on ice sheet dynamics at the Mid-Pleistocene Transition. *Paleoceanography*, 27(3), PA3214. <https://doi.org/10.1029/2011PA002209>.
- Heward, A.P., 1978. Alluvial fan sequence and megasequence models: With example from Westphalian D – Stephanian B coalfields, Northern Spain. *Fluvial Sedimentology. Memoir of Canadian Society of Petroleum Geologists*, 5, 669–702.

- Holmes, A., 1965. *Principles of Physical Geology*. Ronald, New York, pp. 1–1288.
- Hooke, R.L., 1967. Processes on arid-region alluvial fans. *The Journal of Geology*, 75(4), 438–460. <https://doi.org/10.1086/627271>.
- Horváth, F., 1995. Phases of compression during the evolution of the Pannonian Basin and its bearing on hydrocarbon exploration. *Marine and Petroleum Geology*, 12(8), 837–844. [https://doi.org/10.1016/0264-8172\(95\)98851-U](https://doi.org/10.1016/0264-8172(95)98851-U).
- Ivković, Ž., Matej, S., Škoko, M., 2000. Seismostratigraphic interpretation of Upper Miocene and Pliocene sediments of the Sava depression. In: Vlahović, I., Biondić, R. (Eds.), *Proceedings of the Second Croatian Geological Congress*, pp. 219–222. Cavtat, May 17–20, 2000.
- Jamičić, D., 1983. Strukturni sklop metamorfnih stijena Krndije i južnih padina Papuka (Structural fabric of the metamorphosed rocks of Mt. Krndija and the eastern part of Mt. Papuk). *Zagreb Geoloski Vjesnik*, 36, 51–72 (in Croatian).
- Jamičić, D., 1995. The role of sinistral strike-slip faults in the formation of the structural fabric of the Slavonian Mts. (Eastern Croatia). *Geologia Croatica*, 48(2), 155–160. <https://doi.org/10.4154/GC.1995.12>.
- Jamičić, D., Brkić, M., Crnko, J., Vragović, M., 1987. *Basic Geological Map of Yugoslavia, Scale 1:100 000, Sheet Oraštica*. Geološki Institut, Zagreb. Federalni Geološki Institut Beograd.
- Japundžić, S., Vrsaljko, D., Bortek, Ž., Japundžić, D., Sremac, J., Bošnjak, M., 2017. Dolphin remains (Cetacea: Odontoceti) from the Middle Miocene (Sarmatian) deposits near Našice, Croatia. In: *Abstracts Book: 7th International Workshop Neogene of Central and South-Eastern Europe*. Horvat, Marija; Wacha, Lara (ur.). Zagreb: Hrvatsko geološko društvo, pp. 27–28 (poster).
- Kazár, E., 2005. A new kentriodontid (Cetacea: Delphinoidea) from the Middle Miocene of Hungary. *Fossil Record*, 8(1), 53–73. <https://doi.org/10.5194/fr-8-53-2005>.
- Kazár, E., 2006. *Sophianaecetus*, a replacement name for *Mediocris* (Cetacea: Delphinoidea: Kentriodontidae). *Fossil Record*, 9(2), 260. <https://doi.org/10.5194/fr-9-260-2006>, 260.
- Kazár, E., Venczel, M., 2003. Kentriodontid remains (Cetacea: Odontoceti) from the Middle Miocene of Bihor County, Romania. *Nymphaea*, 39–66.
- Kováč, M., Halássová, E., Hudáčková, N., Holcová, K., Hyžný, M., Jamrich, M., Ruman, A., 2018. Towards better correlation of the Central Paratethys regional time scale with the standard geological time scale of the Miocene Epoch. *Geologica Carpathica*, 69(3), 283–300. <https://doi.org/10.1515/geoca-2018-0017>.
- Kováč, M., Márton, E., Oszczypko, N., Vojtko, R., Hók, J., Králiková, S., Plašienka, D., Klučiar, T., Hudáčková, N., Oszczypko-Clowes, M., 2017. Neogene palaeogeography and basin evolution of the Western Carpathians, Northern Pannonian domain and adjoining areas. *Global and Planetary Change*, 155, 133–154. <https://doi.org/10.1016/j.gloplacha.2017.07.004>.
- Kovačić, M., Grizelj, A., 2006. Provenance of the Upper Miocene clastic material in the southwestern part of the Pannonian Basin. *Geologica Carpathica*, 57(6), 495–510.
- Kovačić, M., Zupanić, J., Babić, L., Vrsaljko, D., Miknić, M., Bakrač, K., Hećimović, I., Avanić, R., Brkić, M., 2004. Lacustrine basin to delta evolution in the Zagorje Basin, a Pannonian sub-basin (Late Miocene: Pontian, NW Croatia). *Facies*, 50(1), 19–33. <https://doi.org/10.1007/s10347-003-0001-6>.
- Krkalo, E., 1998. In: Pamić, J. (Ed.), *Ležišta neogenskih kvarcnih pijesaka u rubnim područjima slavonskih planina (Hrvatska)*. Institut za geološka istraživanja, Zagreb, pp. 1–174.
- Kuhle, A.J., Smith, G.A., 2001. Alluvial-slope deposition of the Skull Ridge Member of the Tesuque Formation, Española Basin, New Mexico. *New Mexico Geology*, 23(2), 30–37. <https://doi.org/10.58799/NMG-v23n2.30>.
- Kurečić, T., Kovačić, M., Grizelj, A., 2021. Mineral assemblage and provenance of the Pliocene *Viviparus* beds from the area of Vukomeričke Gorice, Central Croatia. *Geologia Croatica*, 74(3), 253–271. <https://doi.org/10.4154/gc.2021.16>.
- Lewis, D.W., McConchie, D., 2012. *Analytical Sedimentology*. Springer, Dordrecht.
- Magyar, I., 1995. Late Miocene mollusc biostratigraphy in the eastern part of the Pannonian Basin (Tiszantúl, Hungary). *Geologica Carpathica*, 46(1), 29–36.
- Magyar, I., Radivojević, D., Sztanó, O., Synak, R., Ujszászi, K., Pócsik, M., 2013. Progradation of the paleo-Danube shelf margin across the Pannonian Basin during the Late Miocene and Early Pliocene. *Global and Planetary Change*, 103, 168–173. <https://doi.org/10.1016/j.gloplacha.2012.06.007>.
- Mahaney, W.C., 2002. *Atlas of Sand Grain Surface Textures and Applications*. Oxford University Press, New York, pp. 1–237.
- Mahaney, W.C., Vaikmae, R., Vares, K., 1991. Scanning electron microscopy of quartz grains in supraglacial debris, Adishy Glacier, Caucasus Mountains. *U.S.S.R. Boreas*, 20, 395–404.
- Mandić, O., Kurečić, T., Neubauer, T.A., Harzhauser, M., 2015. Stratigraphic and palaeogeographic significance of lacustrine molluscs from the Pliocene *Viviparus* beds in central Croatia. *Geologia Croatica*, 68(3), 179–207. <https://doi.org/10.4154/gc.2015.15>.
- Mange, M.A., Maurer, H.F.W., 1992. Heavy mineral descriptions and colour plates. In: *Heavy Minerals in Colour*. Springer, Dordrecht. https://doi.org/10.1007/978-94-011-2308-2_7.
- Márton, E., Pavelić, D., Tomljenović, B., Pamić, J., Márton, P., 1999. First paleomagnetic results on Tertiary rocks from the Slavonian Mountains in the southern Pannonian Basin, Croatia. *Geologica Carpathica*, 50(3), 273–279.
- Marx, F.G., Lambert, O., Uhen, M.D., 2016. *Cetacean Paleobiology*. John Wiley and Sons, Chichester, U.K., pp. 1–319.
- Maslin, M.A., Brierley, C.M., 2015. The role of orbital forcing in the Early Middle Pleistocene Transition. *Quaternary International*, 389, 47–55. <https://doi.org/10.1016/j.quaint.2015.01.047>.
- Matošević, M., Marković, F., Bigunac, D., Šuica, S., Krizmanić, K., Perković, A., Kovačić, M., Pavelić, D., 2023. Petrography of the Upper Miocene sandstones

- from the North Croatian Basin: Understanding the genesis of the largest reservoirs in the southwestern part of the Pannonian Basin System. *Geologica Carpathica*, 74(2), 155–179. <https://doi.org/10.31577/GeolCarp.2023.06>.
- McKenna, J.P., Santi, P.M., Amblard, X., Negri, J., 2012. Effects of soil-engineering properties on the failure mode of shallow landslides. *Landslides*, 9(2), 215–228. <https://doi.org/10.1007/s10346-011-0295-3>.
- Merchel, S., Beutner, S., Opel, T., Rugel, G., Scharf, A., Tiessen, C., Weiß, S., Wetterich, S., 2019. Attempts to understand potential deficiencies in chemical procedures for AMS. *Nuclear Instruments and Methods in Physics Research Section B: Beam Interactions with Materials and Atoms*, 456, 186–192. <https://doi.org/10.1016/j.nimb.2019.05.005>.
- Merchel, S., Herpers, U., 1999. An update on radiochemical separation techniques for the determination of long-lived radionuclides via accelerator mass spectrometry. *Radiochimica Acta*, 84(4), 215–219. <https://doi.org/10.1524/ract.1999.84.4.215>.
- Miall, A.D., 1996. *The Geology of Fluvial Deposits*. Springer-Verlag, Berlin, Heidelberg, New York, pp. 1–582.
- Mikuž, V., 1999. The great-teeth shark *Carcharocles megalodon* (Agassiz) also from Middle Miocene–Badenian beds above Trbovlje, Slovenia. *Geologija*, 42(1), 141–150. <https://doi.org/10.5474/geologija.1999.008>.
- Müller, J., 1855. *Über die Gattungen der Seeigellarven. Siebte Abhandlung über die Metamorphose der Echinodermen*. Berlin, Druckerei der Königl. Akademie der Wissenschaften. <https://doi.org/10.5962/bhl.title.11344>.
- Mutti, E., Davoli, G., Tinterri, R., Zavala, C., 1996. The importance of fluvio-deltaic systems dominated by catastrophic flooding in tectonically active basins. *Memorie di Scienze Geologiche*, 48, 233–291.
- Muttoni, G., Ravazzi, C., Breda, M., Pini, R., Laj, C., Kissel, C., Mazaud, A., Garzanti, E., 2007. Magnetostratigraphic dating of an intensification of glacial activity in the southern Italian Alps during Marine Isotope Stage 22. *Quaternary Research*, 67(1), 161–173. <https://doi.org/10.1016/j.yqres.2006.07.006>.
- Nemec, W., Kazanci, N., 1999. Quaternary colluvium in west-central Anatolia: Sedimentary facies and palaeoclimatic significance. *Sedimentology*, 46(1), 139–170. <https://doi.org/10.1046/j.1365-3091.1999.00210.x>.
- Nemec, W., Postma, G., 1993. Quaternary alluvial fans in southwestern Crete: Sedimentation processes and geomorphic evolution. In: Marzo, M., Puigdefábregas, C. (Eds.), *Alluvial Sedimentation*. IAS Special Publications, 17, 235–276.
- Nemec, W., Steel, R.J., 1984. Alluvial and coastal conglomerates: Their significant features and some comments on gravelly mass-flow deposits. In: Coster, E.H., Steel, R.J. (Eds.), *Sedimentology of Gravels and Conglomerates*. Canadian Society of Petroleum Geologists Memoir, 10, 1–31.
- Pavelić, D., 2001. Tectonostratigraphic model for the North Croatian and North Bosnian sector of the Miocene Pannonian Basin System. *Basin Research*, 13(3), 359–376. <https://doi.org/10.1046/j.0950-091x.2001.00155.x>.
- Pavelić, D., Kovačić, M., 2018. Sedimentology and stratigraphy of the Neogene rift-type North Croatian Basin (Pannonian Basin System, Croatia): A review. *Marine and Petroleum Geology*, 91, 455–469. <https://doi.org/10.1016/j.marpetgeo.2018.01.026>.
- Pavelić, D., Kovačić, M., Tibljaš, D., Galić, I., Marković, F., Pavičić, I., 2022. The transition from a closed to an open lake in the Pannonian Basin System (Croatia) during the Miocene Climatic Optimum: Sedimentological evidence of Early Miocene regional aridity. *Palaeogeography, Palaeoclimatology, Palaeoecology*, 586, 110786. <https://doi.org/10.1016/j.palaeo.2021.110786>.
- Pavelić, D., Miknić, M., Šlat, M.S., 1998. Early to Middle Miocene facies succession in lacustrine and marine environments on the southwestern margin of the Pannonian Basin System (Croatia). *Geologica Carpathica*, 49(6), 433–443.
- Piller, W.E., Harzhauser, M., Mandić, O., 2007. Miocene central Paratethys stratigraphy — Current status and future directions. *Stratigraphy*, 4(2–3), 151–168.
- Platt, N.H., Keller, B., 1992. Distal alluvial deposits in a foreland basin setting — The Lower Freshwater Molasse (Lower Miocene), Switzerland: Sedimentology, architecture and palaeosols. *Sedimentology*, 39(4), 545–565. <https://doi.org/10.1111/j.1365-3091.1992.tb02136.x>.
- Rögl, F., Steininger, F.F., 1981. Vom Zerfall der Tethys zu Mediterran und Paratethys. Die neogene Paläogeographie und Palinspastik des zirkum-mediterranen Raumes. *Annalen des Naturhistorischen Museums in Wien. Serie A für Mineralogie und Petrographie, Geologie und Paläontologie. Anthropologie und Prähistorie*, 85, 135–163.
- Royden, L.H., 1988. Late Cenozoic tectonics of the Pannonian Basin System. In: Royden, L.H., Horváth, F. (Eds.), *The Pannonian Basin: A Study in Basin Evolution*. AAPG Memoir, 45, 27–48.
- Ruszkiczay-Rüdiger, Zs., Neuhuber, S., Braucher, R., Lachner, J., Steier, P., Wieser, A., Braun, M., ASTER Team, 2021. Comparison and performance of two cosmogenic nuclide sample preparation procedures of in situ produced ^{10}Be and ^{26}Al . *Journal of Radioanalytical and Nuclear Chemistry*, 329(3), 1523–1536.
- Sabol, M., Joniak, P., Bilgin, M., Bonilla-Solomón, I., Cailleaux, F., Čerňanský, A., Malíková, V., Šedivá, M., Tóth, C., 2021. Updated Miocene mammal biochronology of Slovakia. *Geologica Carpathica*, 72(5), 425–443.
- Saftić, B., Velić, J., Sztanó, O., Juhász, G., Ivković, Z., 2003. Tertiary subsurface facies, source rocks and hydrocarbon reservoirs in the SW part of the Pannonian Basin (northern Croatia and south-western Hungary). *Geologia Croatica*, 56(1), 101–122. <https://doi.org/10.4154/232>.
- Sebe, K., Kovačić, M., Magyar, I., Krizmanić, K., Špelić, M., Bigunac, D., Sütő-Szentai, M., Kovács, Á., Szuromi-Korecz, A., Bakrač, K., Hajek-Tadesse, V., Troškot-Čorbić, T., Sztanó, O., 2020. Correlation of Upper Miocene–Pliocene Lake Pannon deposits across the Drava Basin, Croatia and Hungary. *Geologia Croatica*, 73(3), 177–195. <https://doi.org/10.4154/gc.2020.12>.
- Shanmugam, G., 1996. High-density turbidity currents: Are they sandy debris flows? *Journal of Sedimentary Research*, 66(1), 2–10.
- Smith, G.A., 2000. Recognition and significance of streamflow-dominated piedmont facies in extensional

- basins. *Basin Research*, 12(3–4), 399–411. <https://doi.org/10.1111/j.1365-2117.2000.00125.x>.
- Smoot, J.P., 1983. Depositional subenvironments in an arid closed basin; the Wilkins Peak Member of the Green River Formation (Eocene), Wyoming, U.S.A. *Sedimentology*, 30(6), 801–827. <https://doi.org/10.1111/j.1365-3091.1983.tb00712.x>.
- Song, Y., Guo, Z.T., Marković, S., Hambach, U., Deng, C.L., Chang, L., Wu, J.Y., Hao, Q.Z., 2018. Magnetic stratigraphy of the Danube loess: A composite Titel-Stari Slankamen loess section over the last one million years in Vojvodina, Serbia. *Journal of Asian Earth Sciences*, 155, 68–80. <https://doi.org/10.1016/j.jseaes.2017.11.012>.
- Steier, P., Martschini, M., Buchriegler, J., Feige, J., Lachner, J., Merchel, S., Michlmayr, L., Priller, A., Rugel, G., Schmidt, E., Wallner, A., Wild, E.M., Golser, R., 2019. Comparison of methods for the detection of ^{10}Be with AMS and a new approach based on a silicon nitride foil stack. *International Journal of Mass Spectrometry*, 444, 116175. <https://doi.org/10.1016/j.ijms.2019.116175>.
- Šujan, M., Braucher, R., Mandić, O., Fordinál, K., Brixová, B., Pipík, R.K., Šimo, V., Jamrich, M., Rybár, S., Klučiar, T., ASTER Team, Ruman, A., Zvara, I., Kováč, M., 2021b. Lake Pannon transgression on the westernmost tip of the Carpathians constrained by biostratigraphy and authigenic $^{10}\text{Be}/^9\text{Be}$ dating (central Europe). *Rivista Italiana di Paleontologia e Stratigrafia*, 127(3), 627–653. <https://doi.org/10.13130/2039-4942/16620>.
- Šujan, M., Braucher, R., Šujan, M., Hók, J., Povinec, P.P., Šipka, F., Aster, Team, Rugel, G., Scharf, A., 2019. The tectono-sedimentary evolution of a major seismogenic zone with low slip rate activity: A geochronological and sedimentological investigation of the Dobrá Voda Depression (Western Carpathians). *Sedimentary Geology*, 383, 248–267. <https://doi.org/10.1016/j.sedgeo.2019.02.003>.
- Šujan, M., Rybár, S., Kováč, M., Bielik, M., Majcin, D., Minár, J., Plašienka, D., Nováková, P., Kotulová, J., 2021a. The polyphase rifting and inversion of the Danube Basin revised. *Global and Planetary Change*, 196, 103375. <https://doi.org/10.1016/j.gloplacha.2020.103375>.
- Šujan, M., Rybár, S., Thamó-Bozsó, E., Klučiar, T., Tibenský, M., Sebe, K., 2022. Collapse wedges in periglacial eolian sands evidence Late Pleistocene paleoseismic activity of the Vienna Basin Transfer Fault (western Slovakia). *Sedimentary Geology*, 431, 106103. <https://doi.org/10.1016/j.sedgeo.2022.106103>.
- Tomljenović, B., Csontos, L., 2001. Neogene–Quaternary structures in the border zone between Alps, Dinarides and Pannonian Basin (Hrvatsko Zagorje and Karlovac basins, Croatia). *International Journal of Earth Sciences*, 90(3), 560–578. <https://doi.org/10.1007/s005310000176>.
- Vos, K., Vandenberghe, N., Elsen, J., 2014. Surface textural analysis of quartz grains by scanning electron microscopy (SEM): From sample preparation to environmental interpretation. *Earth-Science Reviews*, 128, 93–104. <https://doi.org/10.1016/j.earscirev.2013.10.013>.
- Vrbanac, B., 2002. Facies and facies architecture of the Ivanic Grad Formation (upper Pannonian) — Sava Depression, NW Croatia. *Geologia Croatica*, 55(1), 57–77. <https://doi.org/10.4154/GC.2002.06>.
- Vrsaljko, D., Japundžić, S., Kovačić, M., Grganić-Vrdoljak, Z., Pleše, P., 2010. Vranić: Najznačajnije nalazište fosilnih kitova u Sjevernoj Hrvatskoj. In: Horvat, M. (Ed.), *Abstracts Book*. Hrvatski geološki institut, Zagreb, p. 118 (poster).
- Wentworth, C.K., 1922. A scale of grade and class terms for clastic sediments. *The Journal of Geology*, 30(5), 377–392. <https://doi.org/10.1086/622910>.
- Wetzel, K.F., Sass, O., Restorff, C., 2006. Mass movement processes in unconsolidated Pleistocene sediments — A multi-method investigation at the "hochgraben" (Jenbach/Upper Bavaria) (Massenbewegungen in pleistozänen Lockersedimenten — eine Untersuchung mit verschiedenen Methoden am Hochgraben (Jenbach/Oberbayern). *Erdkunde*, 60, 246–250.

Supplementary data

Supplementary Tables S1–S4, and CRN to this article can be found online at <https://doi.org/10.1016/j.jop.2024.04.001>.